UC Riverside
UC Riverside Electronic Theses and Dissertations

Title

Nonplanar Three Dimensional Paper Microfluidics And Distance-Based Semi-Quantitative DNA Detection

Permalink

Author

Kalish, Brent Nathaniel

Publication Date

2015

Peer reviewed|Thesis/dissertation

UNIVERSITY OF CALIFORNIA
RIVERSIDE

Nonplanar Three Dimensional Paper Microfluidics And Distance-Based Semi-
Quantitative DNA Detection

A Thesis submitted in partial satisfaction
of the requirements for the degree of

Master of Science

in

Mechanical Engineering

by

Brent Nathaniel Kalish

August 2015

Thesis Committee:
Dr. Hideaki Tsutsui, Chairperson
Dr. Masaru Rao
Dr. Marko Princevac

The Thesis of Brent Nathaniel Kalish is approved:

Committee Chairperson

University of California, Riverside

ABSTRACT OF THE THESIS

Nonplanar Three Dimensional Paper Microfluidics And Distance-Based Semi-Quantitative DNA Detection

by

Brent Nathaniel Kalish

Master of Science, Graduate Program in Mechanical Engineering
University of California, Riverside, August 2015
Dr. Hideaki Tsutsui, Chairperson

The development of patterning high-resolution microfluidic circuits onto cellulose paper in 2007 initiated widespread research into the use of the paper as a low-cost, easy-to-use alternative substrate over the glass and plastics of traditional microfluidics. Paper, as a porous hydrophilic material, naturally wicks fluid through itself, without the need to external pumps or power sources. The patterning of paper into hydrophobic and hydrophilic regions, now achievable with consumer-grade office printers, allowed the design of new 2D devices, capable of multi-analyte detection. 3D devices, made from multiple stacked layers of paper, offer even more possibilities for complex, multi-fluid routing in smaller overall device footprints. The use of patterned aerosol adhesives are investigated as an improved method of attaching multiple paper layers together rapidly and with minimal interference of interlayer fluid transport. Patterned aerosol adhesives also enable the development of nonplanar 3D devices, which represent a novel platform upon which to develop new microfluidic devices, which would otherwise be impossible to construct or function in a planar device.

Much of paper microfluidics research is focused on developing more sophisticated detection methods that provide quantitative data, instead of simple colorimetric qualitative yes/no answers. Frequently quantification is obtained by scanning the device and performing a color intensity analysis to relate a color change to concentrations of a target analyte. This technique suffers due to variations in the quality of imaging equipment and the ambient lighting conditions during image acquisition. To address this, some have proposed distance-based lateral flow devices, where the distance traveled by a colored substance is proportional to the target analyte concentration. The use of a microsphere aggregation-based sandwich assay was investigated for semi-quantitatively determining the concentration of a target ssDNA strand.

Table of Contents

LIST OF FIGURES

LIST OF TABLES

Chapter 1: Paper-Based Microfluidics

INTRODUCTION

Over the past eight years, considerable attention has been paid to the field of paper-based microfluidics for its promises of providing low-cost, point-of-care (POC) diagnostic devices, which require minimal instruction to use.[1-4] These devices often offer similar functionality of other glass and plastic based microfluidic devices at a fraction of the cost. Such devices meet many of the WHO's ASSURED[5] (Affordable, Sensitive, Specific, User-friendly, Robust and rapid, Equipment-free, and Delivered) criteria, developed to detail ideal diagnostic device specifications for use in developing countries.

PAPER

Paper is an incredibly abundant and widely available resource that has a number of properties that make it ideal for use as a microfluidic substrate. One of the primary advantages is that paper is a self-wicking material due to its porous capillary-like structure. This means that external pumps and power sources are not required to drive fluid through a paper-based device, unlike those made of plastics or glass. This makes paper-based devices much easier to use. Paper is also an inexpensive material, an attribute that encourages a robust prototyping and design process and is ideal for use in resource-limited settings, such as those found in developing countries or space. Finally, paper substrates are easy to pattern. There are a number of different methods used to define channels through which fluid will flow; however, most of these methods involve making hydrophilic channels with hydrophobic walls. These methods do limit the devices to use with aqueous solutions only, however, as nonpolar solvents will not be confined to the defined channels.

PATTERNING METHODS

Paper-patterning techniques can be broadly classified into two major categories based on how they create hydrophilic channels and hydrophobic barriers. Paper, which is naturally hydrophilic, can be selectively made hydrophobic to define the boundaries of channels, or it can be treated to become completely hydrophobic and the selectively made hydrophilic again. Each technique has its own advantages and disadvantages, primarily dealing with the as of use and patterning resolution.

Embossing

The very first paper microfluidic devices used a heated embossing stamp to transfer paraffin wax from a wax sheet onto cellulose filter paper to define regions for wicking.[6, 7] This technique requires a custom die for each device, making prototyping and design iterations exceedingly time consuming. Further the resolution of devices is limited by the resolution of the die and by how much the molten wax itself wicks through the paper's porous matrix.

Lithography

More recently, high-resolution techniques utilizing UV lithography have created paper-based microfluidic devices that can have feature as small as 200 μm.[8, 9] These lithographic techniques use a UV-curable photoresists (such as SU-8) soaking the entire paper in resist and then exposing the desired hydrophobic regions to UV light to polymerize the resist. The unexposed regions remain unpolymerized and are easily washed away, leaving hydrophilic regions behind. Polymerized photoresist is mechanically brittle and any bending can cause the formation of cracks, rendering the hydrophobic barrier useless.

Printing

Since the advent of lithographically patterned devices, numerous other methods have been developed, many utilizing commercial printing technology.

Ink Jet Printing

Inkjet printers can be used either to selectively de-hydrophobize or to selective hydrophobize paper. To selectively de-hydrophobize, the printer deposits a solvent, such as toluene, to etch paper that has been treated to be completely hydrophobic with polystyrene.[10, 11] This requires multiple passes through the printer to completely etch away the polystyrene. To selectively hydrophobize, the inkjet can be filled with a paper sizing agent, such as AKD.[12, 13] After printing, the paper needs to be heated, and the locations printed will become hydrophobic. This method of inkjet printing is one of the fastest patterning techniques.

Flexographic Printing

Flexographic printing utilize flexible plates to deposit material such as polystyrene to selectively hydrophobize regions of the paper.[14] This technique requires new flexographic plates for each individual pattern; however, flexographic printing is compatible with roll-to-roll printing, enabling mass manufacturing.

Screen Printing

Screen printing is perhaps the simplest printing technique, as it involves just brushing molten wax over a patterned screen onto the paper.[15] The wax penetrates the

paper, forming hydrophobic barriers. This method has the lowest resolution and requires a new screen for each individual pattern, but is the easiest to use.

Wax Printing

Wax printing requires a printer that uses a solid wax-based ink.[16-19] The design is printed onto the paper and then it is heated to melt the wax, forming hydrophobic barriers. This method requires relatively expensive printers, but along with inkjet printing, is one of the fastest patterning methods.

Plasma Treatment

By plasma treating paper that has been made completely hydrophobic by using a paper sizing agent such as AKD, regions of the paper can be made hydrophilic again.[12, 20] Alternatively, a one-step plasma treatment has been developed that turns hydrophilic regions exposed to a plasma hydrophobic.[21] Plasma treatment requires a custom mask for each individual design to expose the only the desired regions to the plasma.

Laser Treatment

The use of a CO_2 laser can etch the surface of hydrophobic paper, forming hydrophilic channels.[22] Unlike other patterning techniques, this only lets the fluid flow over the paper, not through it. Additionally, to make the fluid wick along the etched channels, silica microparticles need to be deposited into the channels.

Cutting

The final patterning techniques does not involve making any portion of the paper hydrophobic, it simply involves physically removing regions of the paper. This can be accomplished either with a craft cutter,[23, 24] a CO_2 laser cutter.[25-28] Using a laser cutter is

much faster and results in identical devices every time. Removing material does make the devices more fragile than other patterning techniques.

PAPER DEVICES

Diagnostic Techniques

The primary motivation behind paper microfluidics is to develop diagnostic devices capable of replicating, or developing alternatives to, the techniques used in traditional microfluidics and in other laboratory devices. The most basic microfluidic diagnostic devices are qualitative, that merely indicate the presence of a target analyte above a certain threshold. This is often through a change in color or fluorescence of a region of the device, much like how litmus paper reacts to a change in pH. One of the most frequently cited examples of such a device is the home pregnancy test strip. For the pregnancy test strips, a qualitative result is adequate, as a woman is either pregnant, or not pregnant, there is no middle ground. While quantitative information on the relative concentration of hCG may provide additional information, that is not typically the purpose behind such devices. For other situations, qualitative data is wholly inadequate, such as determining a diabetic patient's current glucose levels, or detecting a patient's current viral load, and so quantitative data is necessary.

While a large array of qualitative devices with increasing detection thresholds could conceivably be designed as a means of obtaining quantitative concentration information, this is impractical for samples that need to be frequently tested or only have small available volumes. Designing devices that give appropriately quantitative data is an ongoing field of research, with a variety of different proposed mechanisms.

Color Analysis

Depending on the mechanism behind the color change, a properly calibrated image analysis can relate the color (or fluorescent) intensity to a quantitative measure of concentration. This method, however, necessitates either a camera or scanner to image the device, as the human eye's color perception is not very sensitive and can vary wildly from person to person. Even among cameras and scanners, there are differences in the capabilities of the imaging sensors and the quality and reproducibility of the images they take is highly dependent on the ambient lighting conditions.

Distance-Based

Distance-based devices are those that display a visual signal whose length can be related to the concentration of a target analyte. This signal can be displayed as an analog[29-33] or digital signal[34-37]. In analog distance-based devices, the length of the visible signal is directly measured and related to target analyte concentration. This is best with reactions that produce a high signal to noise ratio, as the leading edge of the colored signal may not have a clear color transition. Digital distance-based devices, on the other hand, are more akin to a number of qualitative detection regions linked in series, where the number of signal containing regions can be related to target analyte concentration.

Device Architecture

Lateral Flow

By far, the most common paper-based microfluidic devices are lateral flow devices, simple one-dimensional strips of paper.[29, 38-40] Samples are introduced at one end of the device and as it wicks along the paper, it interacts with whatever indicating method is being

used. Lateral flow devices are limited to simple detection chemistries, often for only single analyte detection.

Two-Dimensional (2D)

Two-dimensional devices are capable of multiplexed detection, splitting a single sample into multiple channels, where independent, simultaneous detections can take place.[26, 41] Additionally, devices can integrate multiple inlets and design channel dimensions such that different fluids can be delivered sequentially to a reaction zone, enabling complex, multi-step detections.[42, 43]

Planar Three-Dimensional (3D)

Three-dimensional devices further extend the fluid routing capabilities of paper-based devices by allowing independent channels to cross over one another without any fluid mixing. This can be impossible to achieve in a single plane. Three-dimensional devices are typically constructed of multiple layers of paper and adhesive.[44-47] The earliest devices used laser cut double-sided tape to attach individual layers together.[44] Complex channel routing requires carefully patterned and aligned tape to ensure minimal interference of interlayer fluid transfer. Devices using thick tape require either a cellulose power to fill the gaps between layers[44] or they require the gaps to be closed by inelastically deforming and compressing the paper layers together.[45]

To avoid the patterning and subsequent alignment issues present with using tape, liquid and aerosol adhesives have been used to bind the paper layers together.[46, 47] These methods make device design and construction much faster and simpler. There are,

however, some concerns that the adhesive may inhibit flow between layers or interfere with the detection chemistry.

To avoid those concerns altogether, three-dimensional devices have been constructed without an adhesives at all, using origami principles to fold them from a single piece of paper.[48] These devices require external clamps to ensure the continuous and sufficient interlayer contact needed for proper wicking. This does make these devices somewhat more expensive to manufacture and more difficult to use, as each device requires its own housing. This can be partially mitigated by using reusable enclosures and designing devices to a standard size.

Most recently, three-dimensional devices have been designed within the thickness of a single sheet of paper.[19] This is done by wax printing patterns on both sides of the device and then laminated using hot rollers to only partially melt the wax, forming a network of channels inside the paper. While this method does eliminate the complexity involved with aligning different layers and any potential contamination caused by adhesives, this technique has not yet demonstrated multiple independent channels crossing over one another, instead opting to shunt a single channel between the top and bottom of the paper layer. Further development of this technique is expected.

Chapter 2: Patterned Aerosol Adhesives

INTRODUCTION

Multilayer paper microfluidic devices enable complex fluid routing in a much more compact device footprint than would otherwise be possible in a single layer, such as de-multiplexing one fluid inlet to 64 outlets. Additionally, multilayer devices can route multiple fluids over one another without mixing, a feat impossible in a single layer of paper.

The first planar 3D paper microfluidic devices were constructed of multiple individual paper layers held together with laser-cut double-sided tape.[44] The tape must be carefully aligned with the paper and the holes in the tape are filled with a cellulose powder in order for fluid to travel across the gap between paper layers.[44] This technique means each device must be assembled individually. Other techniques use liquid adhesives applied between each layer, carefully applied to avoid interfering with the fluid channels.[49] This technique becomes increasingly difficult as the size of the devices decrease. To speed the fabrication process of these types of devices, a technique using an aerosol adhesive to quickly assemble sheets of devices simultaneously was proposed. Most recently, multiple layers of toner from a laser printer, combined with a laminator, has been used to permanently bind multiple, pre-patterned paper layers together.[50]

Alternatively, to avoid any potential adhesive interference, a few groups have explored using origami techniques to fabricate planar multilayer 3D devices out of a single sheet of paper without the use of adhesives; however, such devices require an external clamp to ensure that the layers remain in contact.[48, 51, 52] The use of origami folding techniques result in devices that do not require as much time during construction to align sequential layers, because folding along predefined lines will ensure features on adjacent

11

layers are properly aligned. Such devices can be stored in bulk unfolded before use, or unfolded after use to view test results that are displayed internally, conserving potentially limited analyte volume. Internally displayed results also provide a measure of privacy regarding potentially sensitive results.

Foldable card devices have also been proposed that include preloaded reagent pads, allowing individuals without extensive training to use the cards, which are activated by folding and adding the sample solution.[53] However, the cards require multiple sheets of different materials and utilize permanent adhesives, preventing the device from being unfolded.

The use of an aerosol adhesive applied through a stencil was proposed to combine the rapid assembly possible with aerosol adhesives, while minimizing potential adhesive interference and still allowing the device to be unfolded after use.

MATERIALS

Allura red, erioglaucine disodium salt, and tartrazine were purchased from Sigma-Aldrich (St. Louis, MO). Whatman grade no. 4 filter paper was purchased from Fisher Scientific (Waltham, MA). Perforated steel sheets were purchased from Metals Depot (Winchester, KY). Super 77 Multipurpose Spray Adhesive (3M, St. Paul, MN) and Repositionable 75 Spray Adhesive (3M, St. Paul, MN) were purchased from McMaster-Carr (Elmhurst, IL). Devices were printed using a Xerox Colorqube 8880 (Norwalk, CN).

METHODS

Adhesive Comparison

To compare the relative adhesive capabilities of the two adhesives (Super 77 and Repositionable 75) a checkerboard pattern (to provide contrast) was printed, melted and sprayed with both adhesives (Figure 2-1). The adhesives were applied both with and without a stencil (Stencil #1). The papers were folded and compressed, as with previous tests, and left to sit for 3 hours, after which they were unfolded.

Single Layer Device

A 2 mm wide by 20 mm long 1D channel was designed in SolidWorks and printed onto Whatman grade no. 4 filter paper using a solid wax ink printer. The paper was then placed on a hotplate for two minutes at 170°C to allow the wax to penetrate vertically through the paper. A spray adhesive (3M's Repositionable 75 and Super 77) was then applied under varying conditions and was allowed to dry. A layer of single-sided tape was placed across the bottom of the device to prevent fluid leakage during testing. (Figure 2-2)

2-Layer Device

The 2-layer test device patterns were designed in SolidWorks and printed onto Whatman grade no. 4 filter paper using a solid wax ink printer. The devices consisted of a circular sample inlet and outlet on the top layer, with a straight channel connecting the two circles on the bottom layer. Devices were designed such that post-melt dimensions would be scaled to the channel width, with channel length measuring 10x its width, surrounded by a wax border as wide as the channel (Figure

13

2-3). The paper was then placed on a hotplate for two minutes at 170°C to allow the wax to penetrate vertically through the paper. A spray adhesive (3M's Repositionable 75 and Super 77) was then applied under varying conditions, immediately after which the devices were cut out from the sheet, folded in half and compressed between two glass slides by hand. This fabrication process is depicted in Figure 2-4. In addition, a layer of single-sided tape was placed across the bottom of the device to prevent fluid leakage during testing.

Effect of Humidity on Storage

To determine the effect ambient humidity has on device lifetime, 2-layer devices with 2 mm channels and adhesive applied through stencil #1 were stored for a week in containers filled with air of different relative humidity levels or dry nitrogen.

4-Layer Device

The 4-layer test device patterns were designed in SolidWorks (adapted from the dimensions provided by Lewis *et al*[46]) and printed onto Whatman grade no. 4 filter paper using a solid wax ink printer. The paper was then placed on a hotplate for two minutes at 170°C to allow the wax to penetrate vertically through the paper. A spray adhesive (3M's Repositionable 75 and Super 77) was then applied under varying conditions. Two different styles of the 4-layer devices were designed. One style was designed such that a single device could be folded in an accordion pleat from a single piece of paper, and the other style was composed of four individual layers of paper. Devices were designed such that post-melt dimensions would result

in 2 mm wide channels in a 2 cm square device. 4 μL of 5 mM dye (red: Allura Red; yellow: tartrazine; blue: erioglaucine disodium salt; green: 10:1 mix of tartrazine:erioglaucine disodium salt) was deposited in each branch (one color per branch) of layer 3 (third layer from the top of the completed device). A layer of single-sided tape was placed across the bottom of the device to prevent fluid leakage during testing. This fabrication process is depicted in Figure 2-6.

Adhesive Application

Adhesive was applied from a distance of 24 cm with spray duration of approximately 1.33 s (or a four-count at 180 bpm), with or without a stencil to create a patterned or uniform layer. The stencils were cleaned using adhesive remover after each set of 10 applications to prevent excess adhesive from blocking the stencils' holes. Stencils ranged from 23% open to 63% open with hole sizes ranging from .0625" to .1875". Table 2-1 lists the details of all the stencils used and depicts the relative hole size differences. The dry mass of the applied adhesive was obtained by applying adhesive to a 9x9 cm square of Whatman grade no. 4 filter paper and waiting 30 minutes for the adhesive to completely dry (Table 2-2).

Data Acquisition and Analysis of Test Devices

All devices were placed inside a sealed, humidity-controlled chamber to isolate them from the effects of wind-induced evaporation during testing. Devices were timed until the wicking fluid reached and fully filled the outlet(s). Devices that did this under the time limit of ten minutes were considered true successes. Devices that did not completely fill the circle or took longer than ten minute were considered partial successes. A cutoff time

of ten minutes was chosen because it was approximately 10 x the longest wicking time of the slowest wicking channel without adhesive. Devices that did not have any fluid reach the outlet were considered failures. A depiction of the different success classifications is shown in Figure 2-7. Wicking time averages were calculated from only true successes.

For the single layer devices, 7 µL of a green colored solution (10:1 mix of 5 mM tartrazine and 5 mM erioglaucine disodium salt in deionized water) was added to the inlet of each device after the applied adhesive had dried. Both adhesives were compared with stencils #1, #5, and no stencil.

For the 2-layer devices, a green colored solution (10:1 mix of 5 mM tartrazine and 5 mM erioglaucine disodium salt in deionized water) was added to the inlet of each device immediately after device assembly. Ten samples of each channel and stencil combination were tested. Wicking fluid volumes were device dimension specific in order to ensure that devices were not supplied with so much fluid that they could not possibly fail. Fluid volumes are shown in Table 2-3.

For the 4-layer devices, 40 µL of deionized water was added to the inlet of each device. Twenty samples of each adhesive application condition were tested.

RESULTS AND DISCUSSION

Adhesive Comparison

When applied without a stencil, adhesive 75 was able to be unfolded without tearing the paper, while with adhesive 77 the paper was torn in half (Figure 2-8A). However, when applied through stencil #1, the 77 performed comparably to the 75, as both were able to be unfolded with ease (Figure 2-8B).

16

Single Layer Device

Figure 2-9 details the effect of the different adhesives and application methods on the wicking in a 1D, single layer channel. Uniform adhesive coverage resulted in much slower wicking than in adhesive-less channels, with adhesive 77 coated channels wicking even slower than in the adhesive 75 coated channels. This agrees with the data obtained from the folded device wicking, in which devices constructed with 77 took longer to wick than those constructed with 75. Both sets of adhesive-covered channels wicked the full length of their channels, unlike with the folded 2 mm devices. When applied through stencil #1, both adhesives had comparable wicking times that fell in-between the wicking times of the adhesive-less 1D channel and the folded devices. The results of this study suggest that inhibited interlayer transfer contributes to diminished wicking success rates and increased wicking times.

2-Layer Device

Adhesive 75

The 2 mm width channel with stencil #1, the least open stencil (23% open) proved to have shortest wicking time among stencils with a 100% true success rate (Figure 2-10). In general, wicking times increased, and success rates fell, as the stencil hole size increased. This is likely due to a higher probability of a stencil hole aligning with the inlet or outlet, resulting in adhesive blocking interlayer flow. In addition, increasing the width of the channel generally increased success rates for most stencils. Further experiments to determine device lifetime, however, proved that the repositionable adhesive lacked the

holding power to extend device viability for much beyond 3 hours, as can be seen in Figure 2-11. The devices endured repeated folding while maintaining high success rates when tested immediately after the repeated folding (Figure 2-12).

Adhesive 77

While devices constructed with 77 had somewhat slower wicking times than those of their 75 counterparts, they all had much higher success rates (Figure 2-13). As with the 75, 77 applied through stencil #1 resulted in devices with standard deviations that were among the lowest out of all channel/stencil combinations. All devices constructed with stencil #1 had a 100% partial success rate, indicating that by increasing wicking fluid volume, 100% true success rates would be achievable.

The same time to failure and repeated folding tests were performed on the devices constructed with adhesive 77 as were previously performed on the adhesive 75 devices. These tests were performed with the 2 mm channel devices, despite having a slower wicking speed than the 1 mm channel, because the 1 mm channel devices were too small to easily manipulate for the required number of folds. Additionally, the dimensions of the 1 mm channel device approach the functional channel width limit obtainable with wax printing methods.[16] The 2 mm channel also had a much smaller deviation in wicking times than the larger channels. As shown in Figure 2-14, the 77 was able to maintain device viability for all ten samples for at least 24 hours after device construction. Devices constructed with 77 could be folded just as many times before being tested, as shown in Figure 2-15. Testing was

performed immediately following the repeated folding, while still within the 77's tack range.

Effect of Humidity on Device Storage

Success rates for the 2-layer devices fell as relative humidity levels increased, with the highest success rates (90%) found when devices were stored under dry nitrogen (Figure 2-16). Such a storage condition, under dry inert gas, is a standard packaging practice for many medical devices and sensitive biological reagents. For longer term storage, or storage under non-ideal conditions, other adhesives (eg. non-hygroscopic) may prove to be more advantageous.

4-Layer Device

Average wicking times and success rates for 4-layer devices constructed with different amounts of applied adhesive are shown in Table 2-4. In stacked devices, uniform adhesive coverage resulted in relatively high success rates that decreased with increasing amounts of adhesive. Patterned adhesive coverage (applied through stencil #1) resulted in very low success rates when adhesive was only applied to one side of the paper, but displayed much higher success rates and faster wicking times when the adhesive was applied to both sides. By doubling the size of the border around the channels (increasing the overall device area by ~30%), success rates for both single- and dual-sided adhesive applications increased. A comparison between the two sizes is shown in Figure 2-17.

In origami folded devices, uniform adhesive coverage resulted in low success rates with complete failure resulting when applying the equivalent amount of adhesive present in the stacked, uniform, single-sided adhesive devices. Patterned adhesive coverage
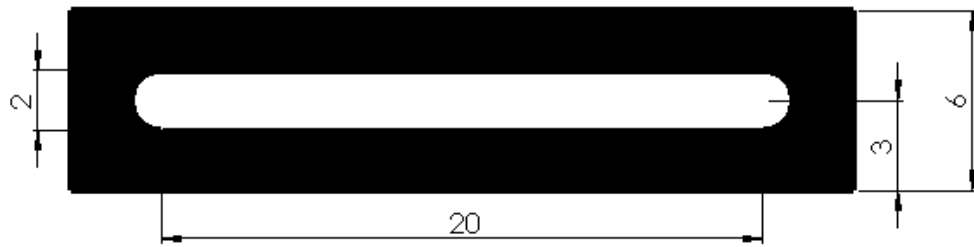
resulted in much lower success rates; however, this decrease was offset by using slightly

larger devices that had 3 mm borders.
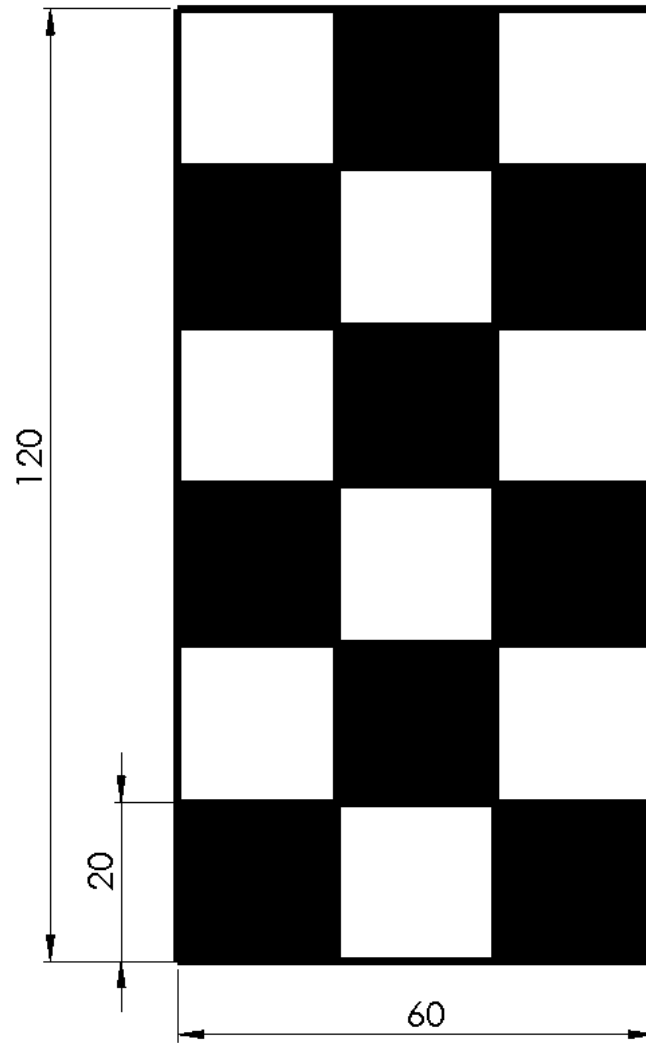
Figure 2-1: Adhesive Comparison Peel Test Dimensions. Checkerboard wax pattern to emphasize any damage caused by unpeeling. The pattern consisted of two 3x3 grids folded onto one another. All dimensions are in mm.
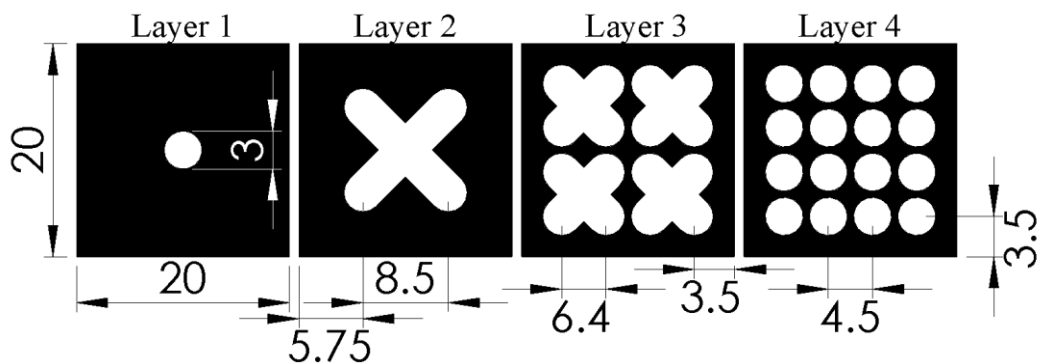
Figure 2-2: Single Layer Device Dimensions. The single layer device contained a channel 2 mm wide and 20 mm long. The wax boundaries around the channel were also 2 mm wide.


Figure 2-3: 2-Layer Device Dimensions. The 2-layer devices are all similar in dimensions. The lower channel is 10 times as long as the channel is wide and all borders are designed to be as thick as the channel is wide after melting.
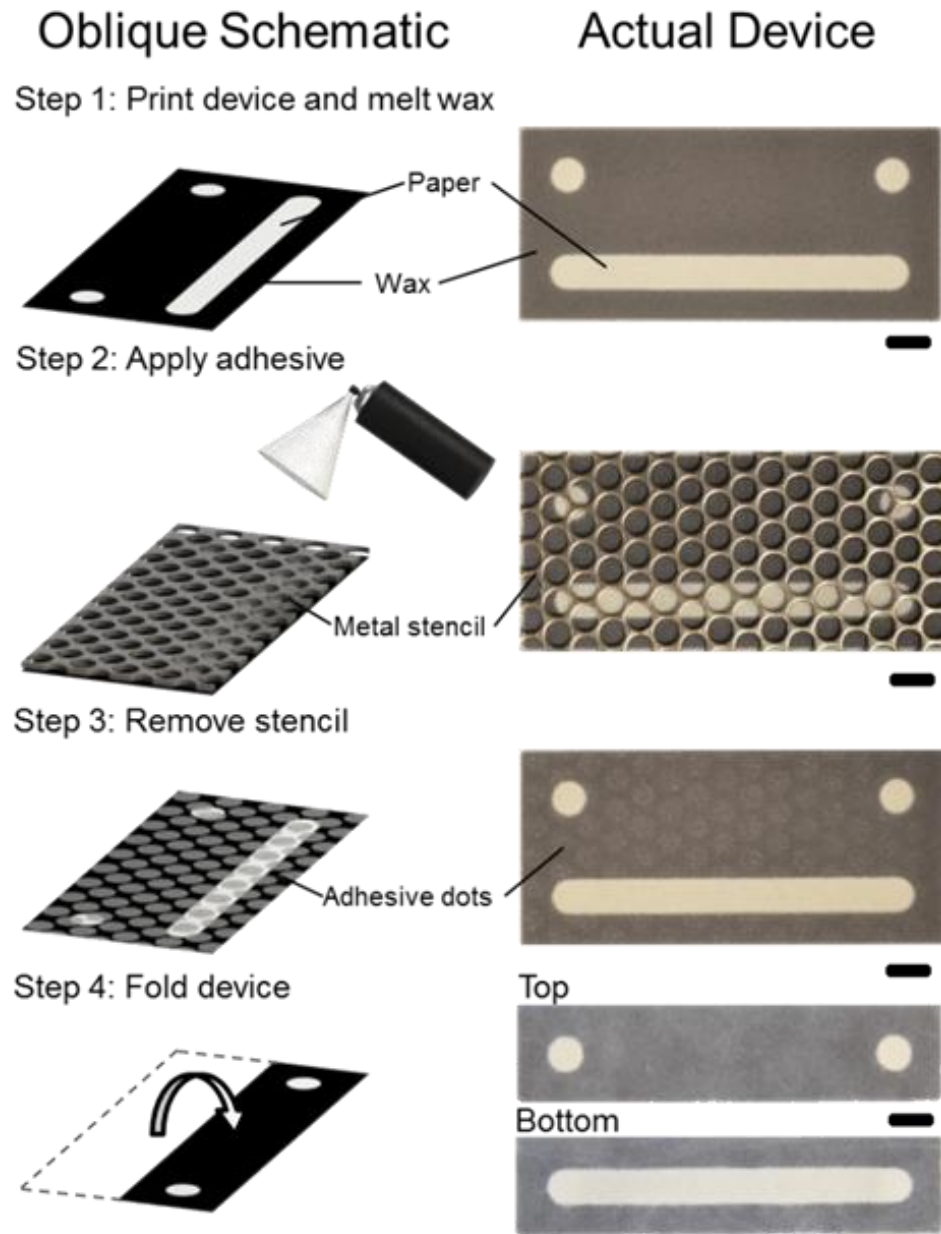
Figure 2-4: 2-Layer Device Fabrication Process. A sheet of devices is printed onto Whatman grade no. 4 filter paper using a solid wax ink printer. The wax is melted on a hotplate for 2 min at 170°C (Step 1). Upon cooling, a spray adhesive is applied through a stencil made of a perforated steel sheet (Step 2), after which the stencil is removed (Step 3) and the device is cut from its sheet and folded (Step 4). All scale bars are 5 mm. (Previously published[54])

Figure 2-5: 4-Layer Device Dimensions. Devices measure 20 mm square and splits a single 3 mm wide inlet on the top layer of the device to 16 outlets on the bottom layer.
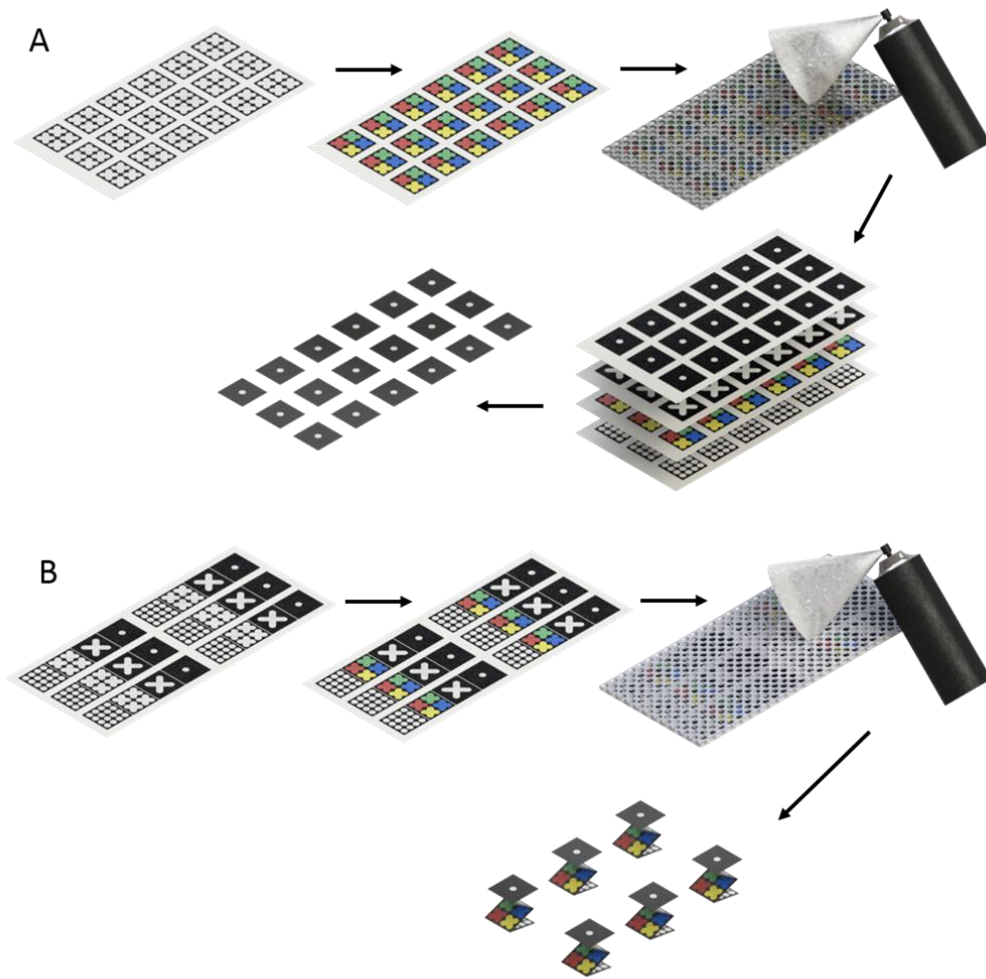
Figure 2-6: 4-Layer Device Fabrication Process. A) Stacked 4-layer device fabrication. B) Origami 4-layer device fabrication. Adhesive was applied to both sides of each sheet, excluding the top of the first layer in the stacked devices.
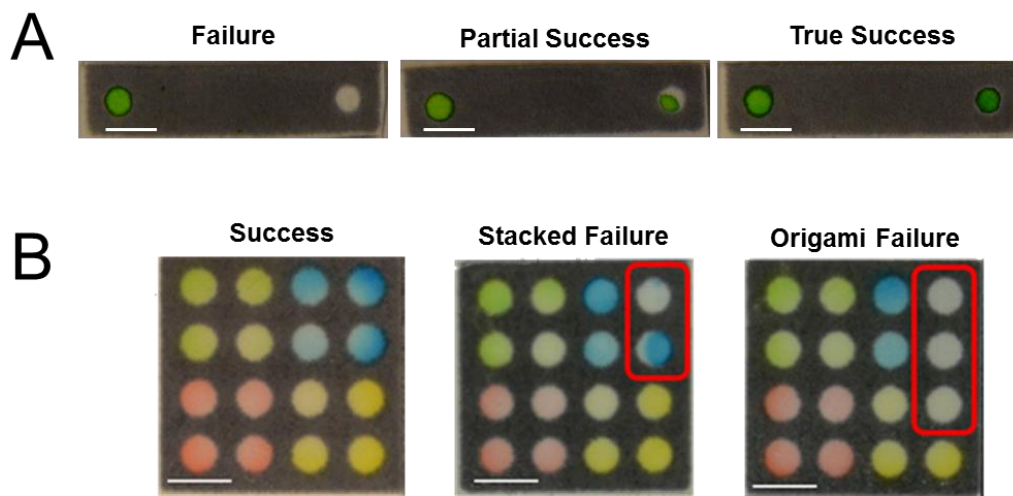
Figure 2-7: 2- and 4-Layer Device Success and Failure Classifications. A) 2-Layer Devices. Device failures are defined as a lack of dye reaching the end. A full success is one in which the outlet circle is completely filled with dye. A partial success is any noticeable amount of dye in the outlet or a full success that took longer than 10 minutes. B) 4-Layer Devices. Success – all outlets completely filled with dye. Typical stacked failure - outlets that failed to completely fill had no apparent pattern in their distribution. Typical origami failure - all outlets that failed to fill were located along the left-most or right-most column, closest to the creases. All scale bars are 5 mm. (Adapted from a previously published figure[54])

A

75 (No Stencil)   77 (No Stencil)

B

75 (With Stencil)   77 (With Stencil)
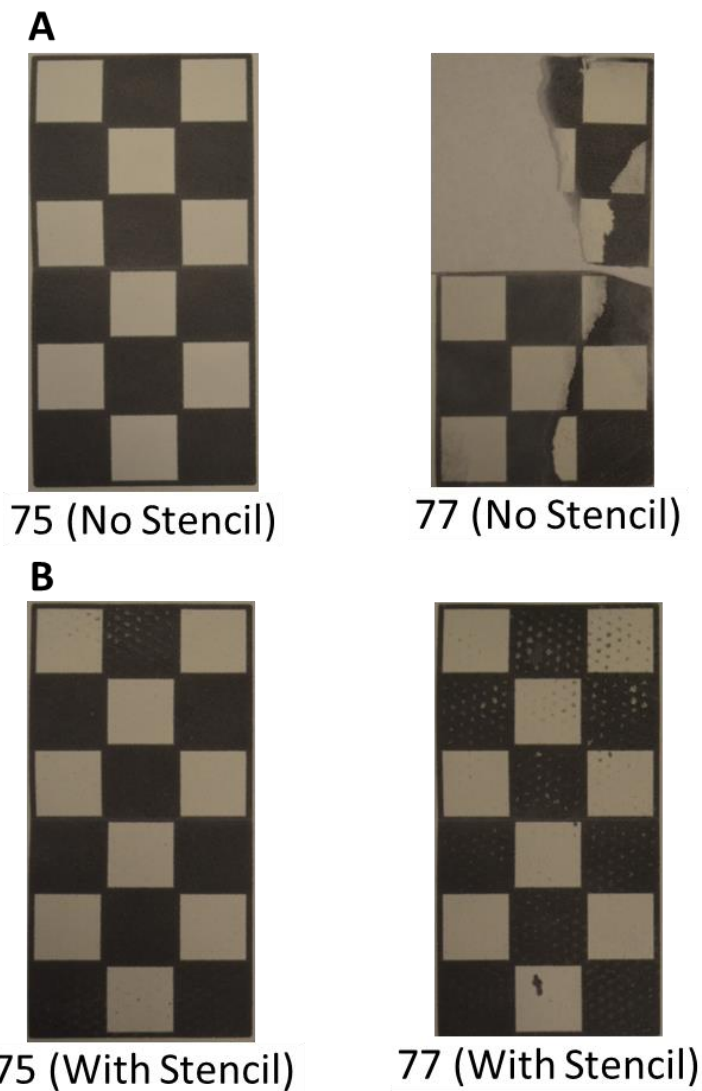
Figure 2-8: Adhesive Comparison Peel Test Results. Peel test comparison of adhesive 75 (Left) and adhesive 77 (Right) 3 hours after adhesive application. A) Adhesive application without a stencil. B) Adhesive application through stencil #1. As expected, without a stencil, adhesive 75 was able to be unfolded without tearing the paper, while adhesive 77 suffered extensive paper damage. However, when applied through stencil #1, both adhesives performed comparably, unfolding with ease. The peel test strips are 60 mm wide and 120 mm long while unfolded. (Previously published[54])
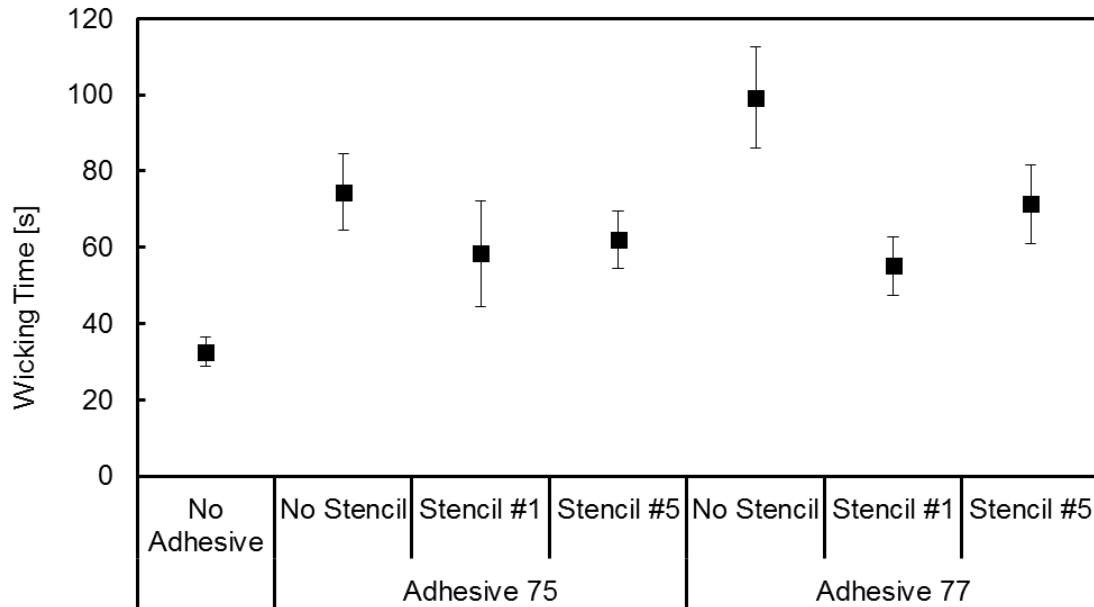
Figure 2-9: Single Layer Device Wicking. Average wicking times in 2 mm wide, 20 mm long, 1D open channels under different adhesive application patterns. N=10. Error bars represent standard deviation. (Previously published[54])
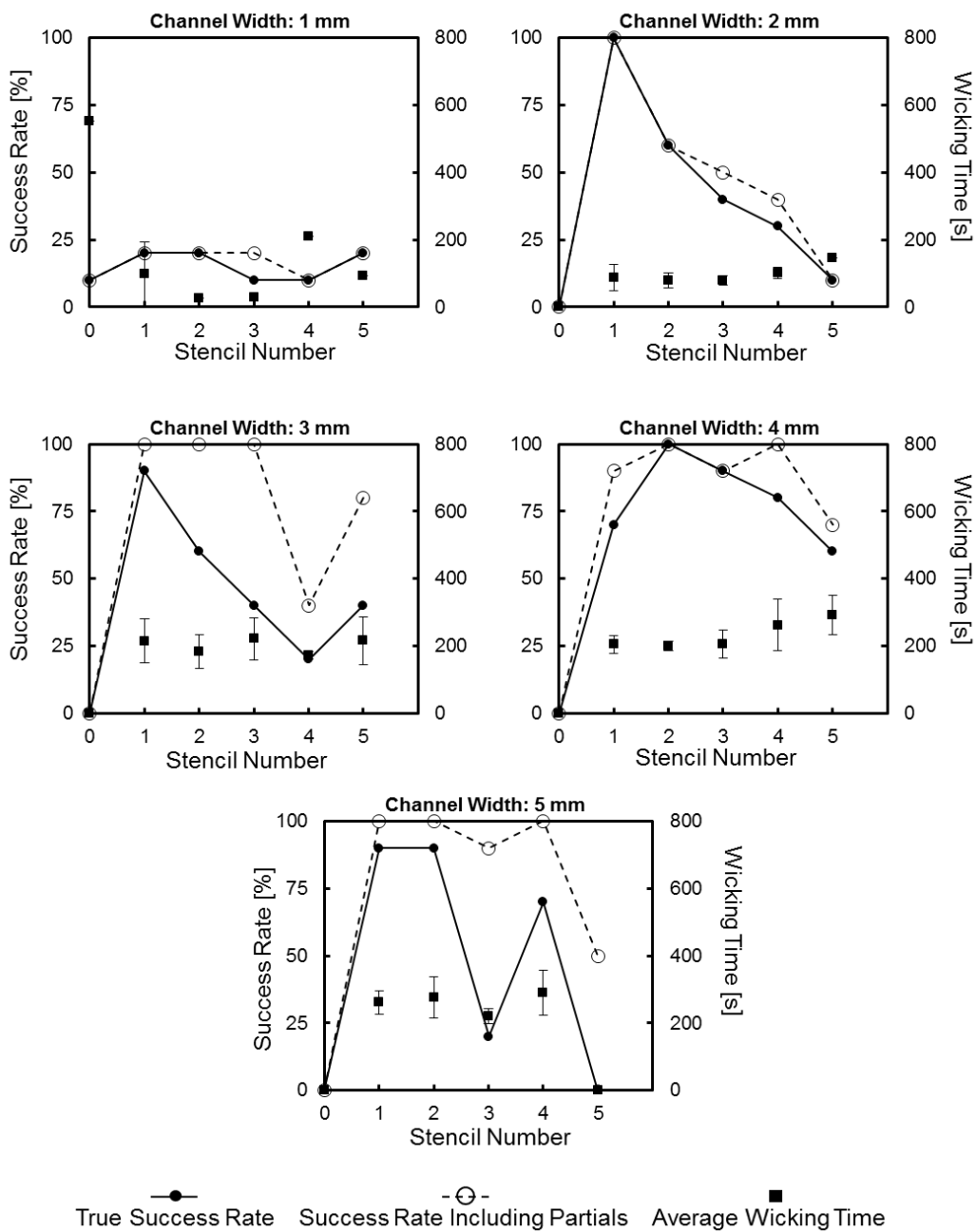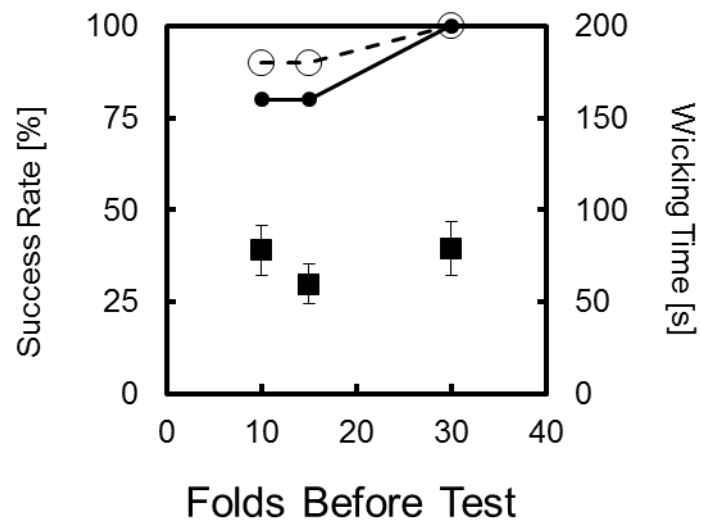
Figure 2-10: 2-Layer Device Wicking – Adhesive 75. Partial and true success rates (primary axis) for each stencil/channel combination and average wicking times (secondary axis) vs. channel width for devices constructed with adhesive 75 for each of the five stencils and the control, no stencil (Stencil #0). N=10. Error bars represent standard deviation.
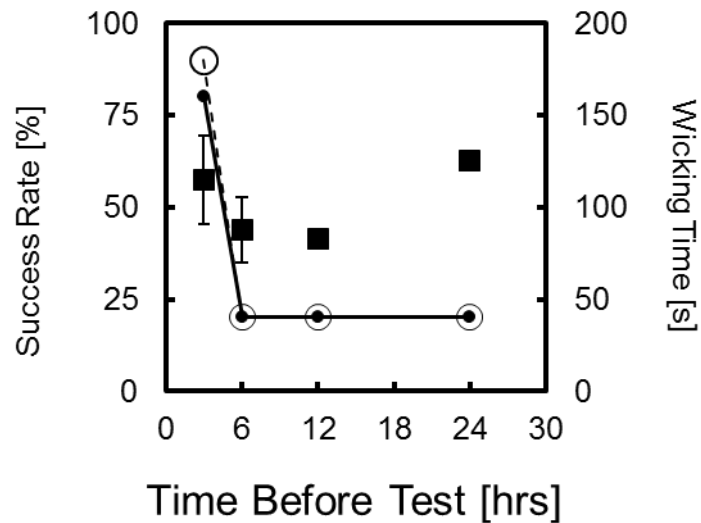
Figure 2-11: **2-Layer Device – Time to Failure – Adhesive 75.** Device success rate and average wicking time vs. time after device assembly for devices with a 2 mm wide channel and adhesive 75 sprayed through stencil #1. N=10. Error bars represent standard deviation. (Previously published[54])

Figure 2-12: 2-Layer Device – Repeated Folding – Adhesive 75. Device success rate and average wicking time vs. repeated folds for devices with a 2 mm wide channel and adhesive 75 sprayed through stencil #1. N=10. Error bars represent standard deviation. (Previously published[54])

Figure 2-13: 2-Layer Device Wicking – Adhesive 77. Partial and true success rates (primary axis) for each stencil/channel combination and average wicking times (secondary axis) vs. channel width for devices constructed with adhesive 77 for each of the five stencils and the control, no stencil (Stencil #0). N=10. Error bars represent standard deviation.
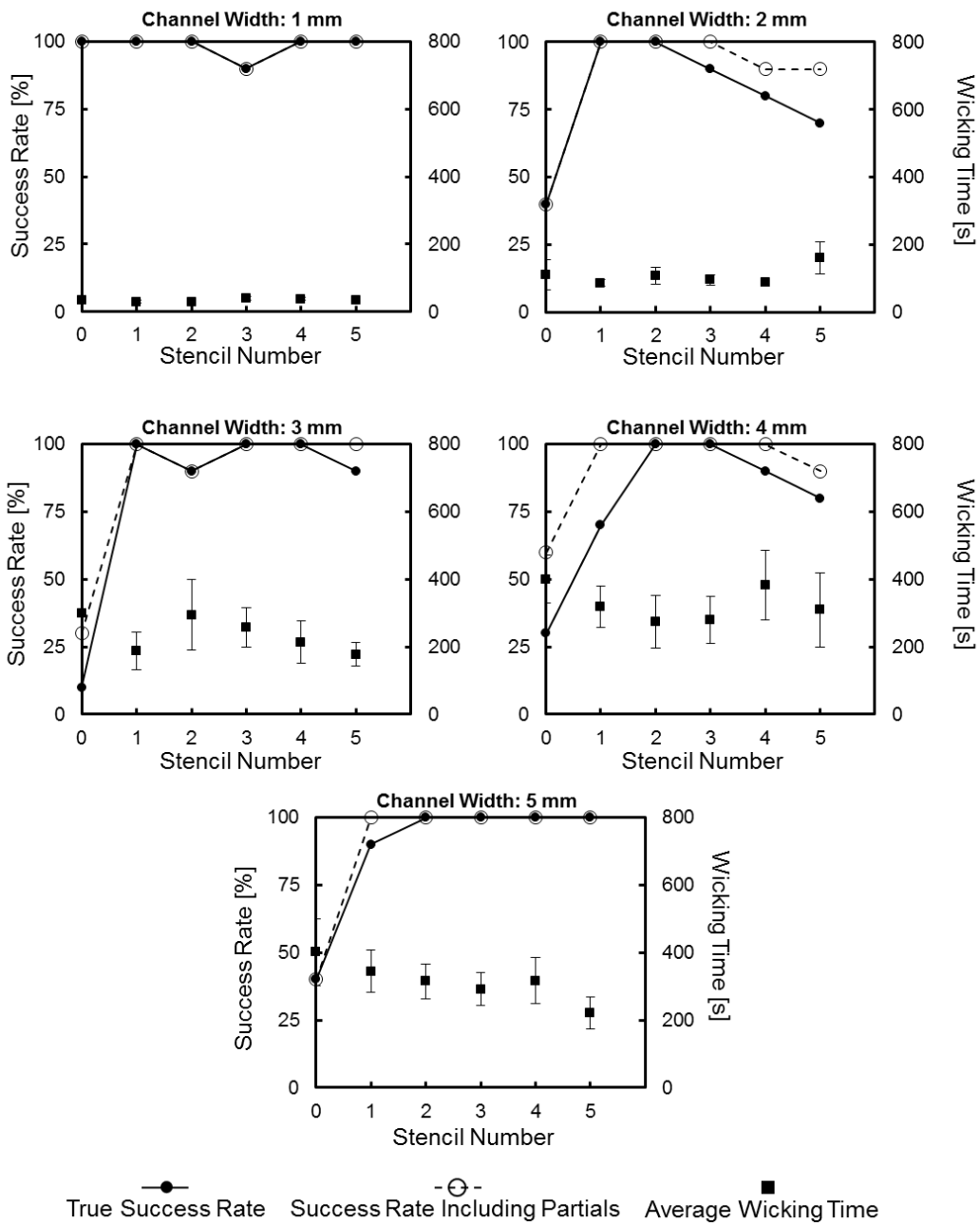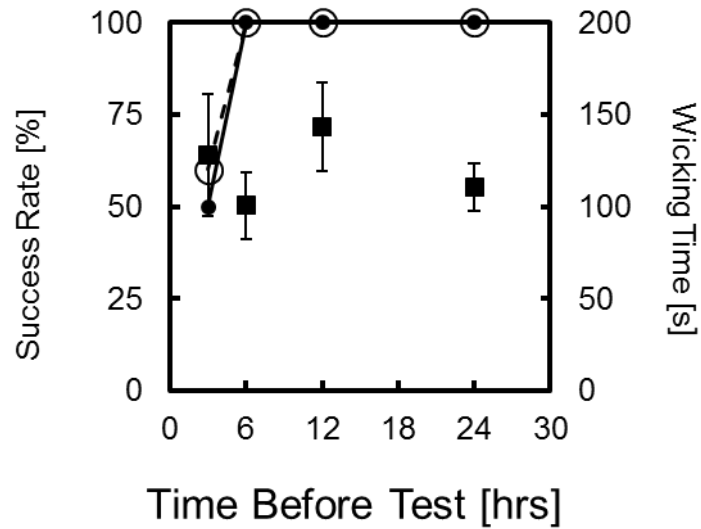
31

Figure 2-14: **2-Layer Device – Time to Failure – Adhesive 77.** Device success rate and average wicking time vs. time after device assembly for devices with a 2 mm wide channel and adhesive 77 sprayed through stencil #1. N=10. Error bars represent standard deviation. (Previously published[54])
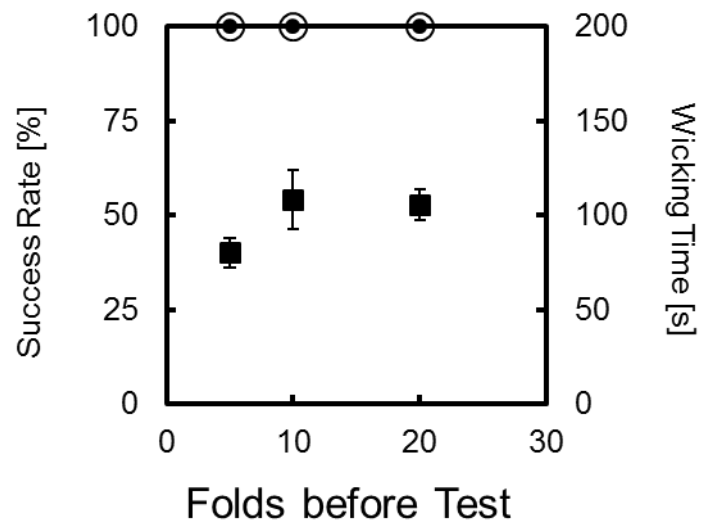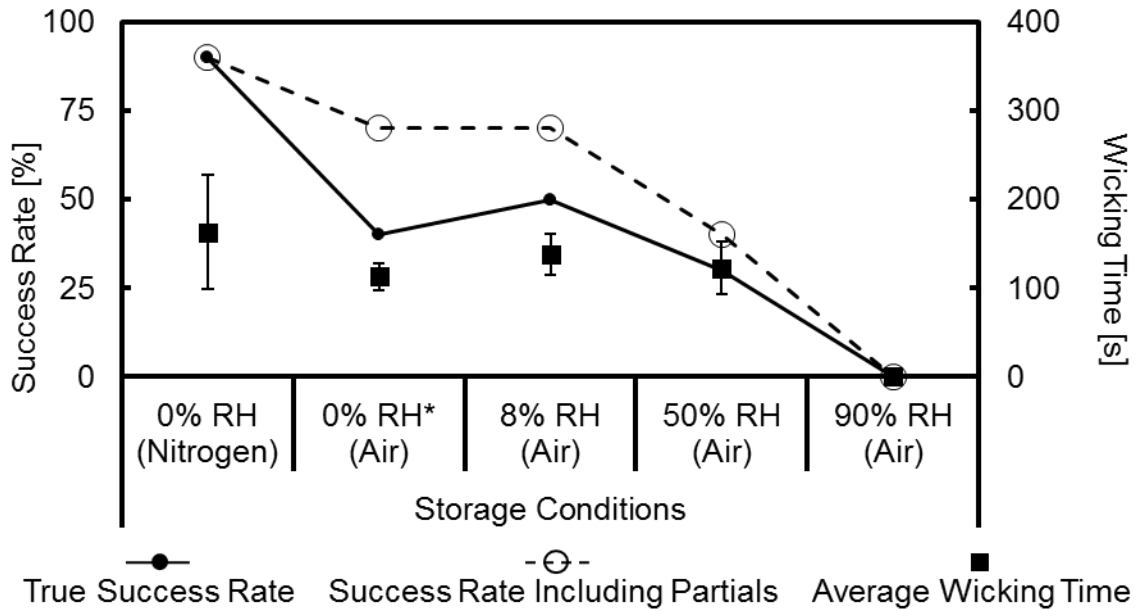

Figure 2-15: 2-Layer Device – Repeated Folding – Adhesive 77. Device success rate and average wicking time vs. repeated folds for devices with a 2 mm wide channel and adhesive 77 sprayed through stencil #1. N=10. Error bars represent standard deviation. (Previously published[54])
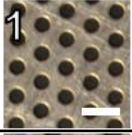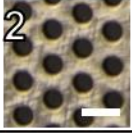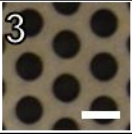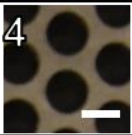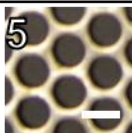
Figure 2-16: 2-Layer Device – Storage Conditions. Success rates and average wicking time of 2 mm channel devices after a week of storage under different relative humidities. N=10. Error bars represent standard deviation. *0% RH (Air) condition is simulated by enclosing 8%RH air in a jar containing desiccant crystals (Drierite, 6 Mesh). (Previously published[54])
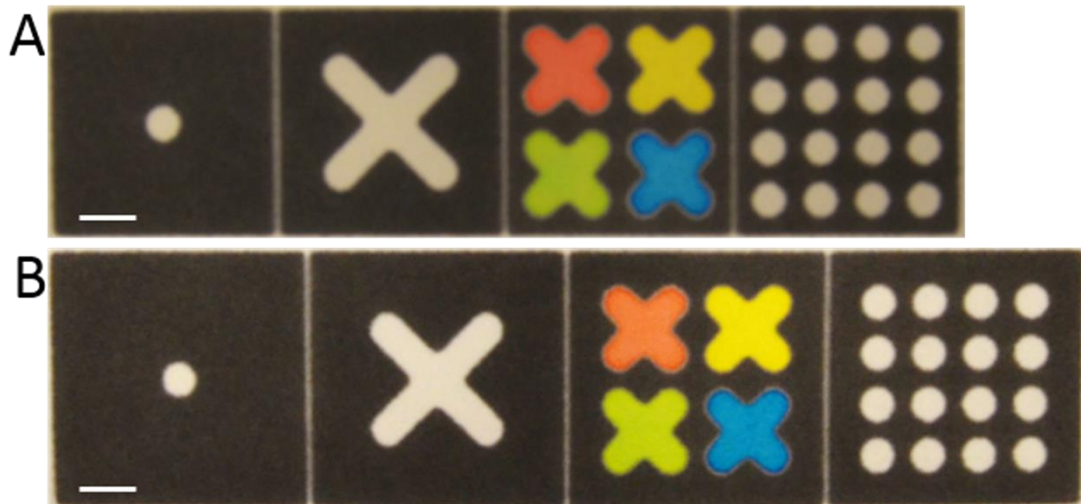
Figure 2-17: 4-Layer Device Size Comparison. A) Smaller device (1.6 mm border). B) Larger device (3 mm border). All scale bars are 5 mm.

.

TABLES

Stencil #	Hole size	Stagger	Percent open	Image
1	1/16 " (1.59 mm)	1/8 " (3.18 mm)	23%	
2	3/32 " (2.38 mm)	5/32 " (3.97 mm)	33%	
3	1/8 " (3.18 mm)	3/16 " (4.76 mm)	40%	
4	3/16 " (4.76 mm)	1/4 " (6.35 mm)	51%	
5	5/32 " (3.97 mm)	3/16 " (4.76 mm)	63%	

Table 2-1: Adhesive Stencil Properties. 1/28" (.91 mm) thick perforated steel sheets used as stencils. All scale bars are 5 mm. (Previously published[54])

Adhesive Coverage	Spray Duration (s)	Average Adhesive (mg/cm²)
Uniform	1	.26 ± .05
Uniform	0.5	.14 ± .03
Patterned	1	.02 ± .01
None	0	-.01 ± .00

Table 2-2: Applied Aerosol Adhesive. Average adhesive thickness (dry mass) of adhesive 77 applied over a 9x9 cm square under different spray conditions. The patterned adhesive was applied through stencil #1. N=10.

Channel Width	Fluid Amount
1 mm	2 µL
2 mm	7 µL
3 mm	15 µL
4 mm	30 µL
5 mm	50 µL

Table 2-3: 2-Layer Device Deposited Fluid Amounts. Fluid amounts used to test each width channel.

Device Style	Adhesive Type (Duration/Border/Sides)	Average ± SD (s)	Success Rate
Origami	Uniform (1.33 s / 1.6 mm / Double)	44 ± 14	45%
	Uniform (0.67 s / 1.6 mm / Double)	0 ± 0	0%
	Patterned (1.33 s / 1.6 mm / Double)	41 ± 13	15%
	Patterned (1.33 s / 3 mm / Double)	64 ± 50	40%
Stacked	Uniform (1.33 s / 1.6 mm / Single)	152 ± 66	80%
	Uniform (1.33 s / 1.6 mm / Double)	119 ± 68	60%
	Patterned (1.33 s / 1.6 mm / Single)	164 ± 75	25%
	Patterned (1.33 s / 1.6 mm / Double)	81 ± 25	80%
	Patterned (1.33 s / 3 mm / Single)	116 ± 63	85%
	Patterned (1.33 s / 3 mm / Double)	80 ± 55	100%

Table2–4: 4-Layer Device Wicking. Average wicking time and success rates for different adhesive application conditions. N=20.

Chapter 3: Nonplanar Three-Dimensional (3D) Paper Microfluidics

INTRODUCTION

In order to expand the technique of patterned adhesive application beyond planar devices, a nonplanar 3D origami structure was chosen to serve as a proof concept. A nonplanar structure would be crushed by the use of any sort of external clamp and the folding order of origami precludes uniform application of a permanent adhesive, because latter steps require unfolding previously made folds. The fluidic circuit within the core of the chosen origami structure was designed using the previously obtained knowledge of adhesive application patterns.

MATERIALS

Allura red, eurioglaucine disodium salt, and tartrazine were purchased from Sigma-Aldrich (St. Louis, MO). Whatman grade no. 4 filter paper was purchased from Fisher Scientific (Waltham, MA). Perforated steel sheets were purchased from Metals Depot (Winchester, KY). Super 77 Multipurpose Spray Adhesive (3M, St. Paul, MN) and Repositionable 75 Spray Adhesive (3M, St. Paul, MN) were purchased from McMaster-Carr (Elmhurst, IL). Devices were printed using a Xerox Colorqube 8880 (Norwalk, CN).

METHODS

Peacock Construction

The origami peacock channel patterns (Figure 3-1) were designed in SolidWorks and printed onto Whatman grade no. 4 filter paper using a solid wax ink printer. The paper was then placed on a hotplate for two minutes at 170°C to allow the wax to penetrate vertically through the paper. The crease pattern[55] (Figure 3-2) was printed onto printer

paper and placed on the hotplate to melt the wax. The crease pattern was aligned and attached to the channel pattern. The crease pattern was traced with a blunt stylus, indenting the pattern into the filter paper.

The crease pattern was then removed from the filter paper and the origami peacock was then folded. Once folded, the peacock was unfolded to expose the portions that required adhesive. Adhesive 77 was applied through masks with and without stencil #1. The peacock was immediately refolded and pressure applied to the adhesive containing region until the adhesive dried.

Wicking

The peacock was placed in a humidity-controlled chamber with a high relative humidity (>90%) to minimize evaporation. Each leg was placed in a container filled with 5 mM dye (red: Allura Red, yellow: tartrazine). One end of a small paper lead (approximately 5 mm wide by 5 cm long) was inserted into the body of the peacock and the other into a container filled with 5 mM dye (blue: erioglaucine disodium salt).

RESULTS AND DISCUSSION

The base origami design is a modified version of Maekawa's[55] peacock. Spray adhesive 77 was applied through stencil #1 (23% open), the stencil that applied the least amount of adhesive in previous tests. A pair of masks were used to apply the patterned adhesive to specific portions of each side of the precreased peacock in order to minimize excess adhesive interfering with folding (Figure 3-3). As shown below in Figure 3-4, three distinct colored fluids were able to wick through the peacock's channels and pass over one another inside the body region without

mixing. The callout in Figure 3-4 shows the direction of blue, yellow, and red solution transport through 3 folded layers without mixing, connecting to three, four, and four channel branches, respectively. A time lapse of this wicking process is shown in Figure 3-5.

In nonplanar 3D structures, uniform adhesive coverage resulted in more difficult folding, as adjacent faces prematurely stuck together. The layers inside the structure cannot be unfolded once the adhesive has dried, and attempts to do so resulted in shredded paper. Patterned adhesive coverage made folding much easier, as any accidental adhesion was easily undone. Once the adhesive dried, the layers could be pulled apart without any ripping or tearing of the paper. Both methods of adhesive application resulted in devices that successfully routed liquid the length of their channels and without mixing; however, the device with uniformly applied adhesive was noticeably slower.

Beyond demonstrating interlayer fluid transfer in a nonplanar 3D structure, the tail of the peacock demonstrates the ability for wicking driven actuation. As the fluid wicks through symmetrically distributed channels, the tail is forced open (Figure 3-5). This opening arises from liquid wicking across folds, where swelling cellulose fibers force open the folds. In addition, the weight of the wicking fluid as it extends outward along the tail, may serve to pull the sides of the tail downwards. These two forces, when coupled with an elastomeric film[56], could form an actuator powered by a fluid wicking along a channel and across strategically placed folds. Once the wicking fluid evaporates, the device would be able to return to its previous configuration. Similar behavior is found in nature, where some seeds (e.g.

40

Pelargonium carnosum), utilize changes in atmospheric humidity to propel themselves into the ground.[57] During periods of low atmospheric humidity, the seed's awn (a seed's fibrous "tail") will dry out; forming a coil, and once atmospheric humidity increases, the hygroscopic awn will straighten out, propelling itself into the ground. It is anticipated that nonplanar 3D paper microfluidic techniques can enable the mimicry of some of nature's designs and functions in novel paper microfluidic devices.

FIGURES
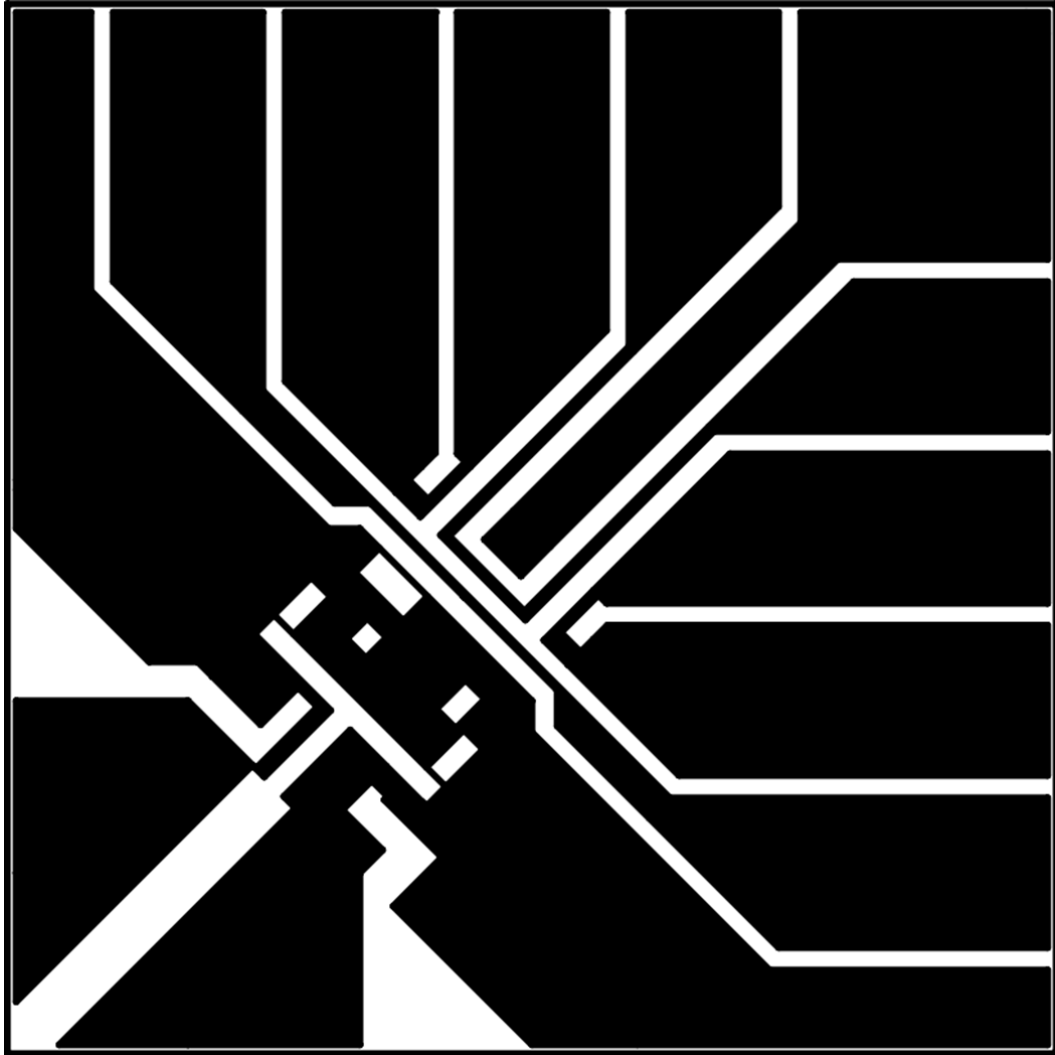
Figure 3-1: Origami Peacock Channel Pattern. Channel pattern, where black indicates hydrophobic regions. Overall pattern is 150 mm square. (Previously published[54])
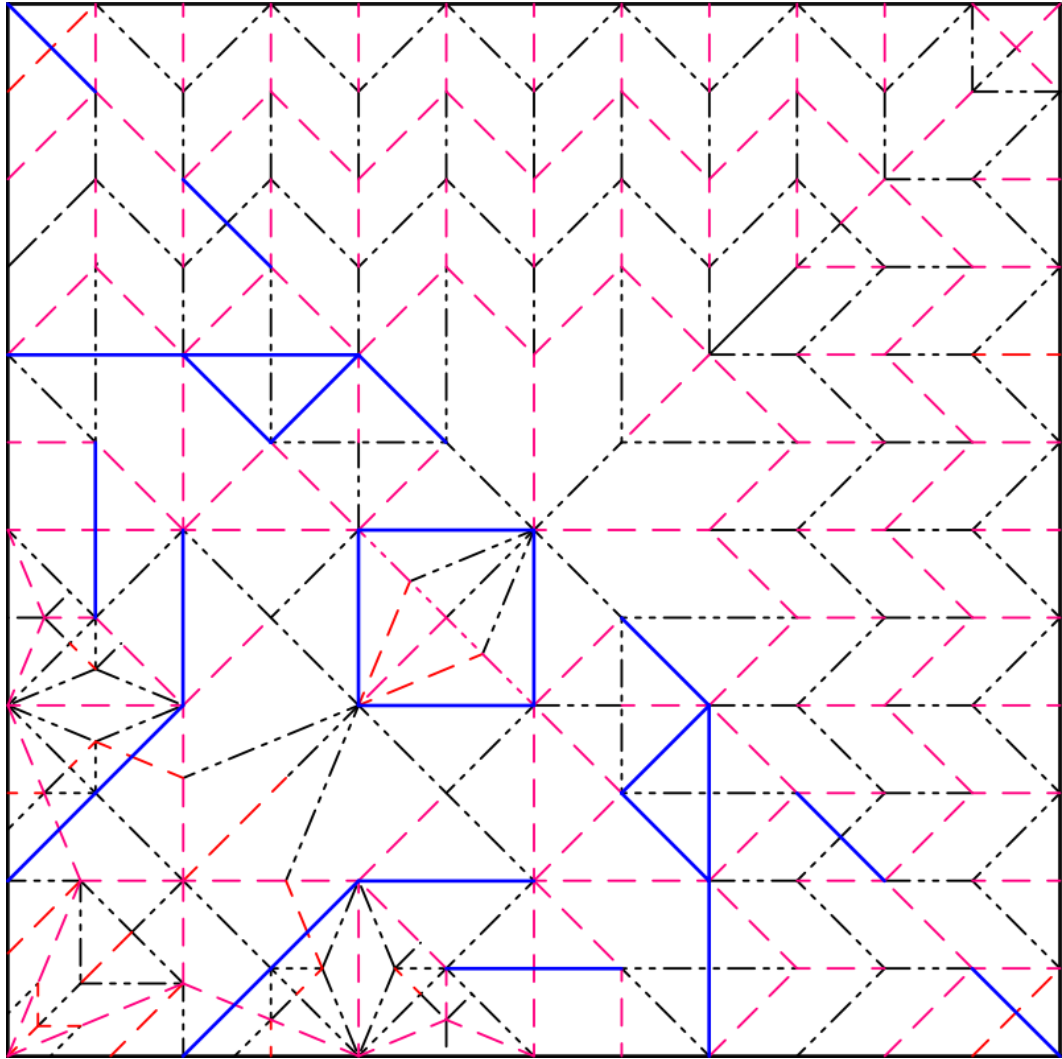
Figure 3-2: Origami Peacock Crease Pattern. Crease pattern modified from [55]. Red lines correspond to mountain folds in the final structure; black lines correspond to valley folds; blue lines correspond to creases that are not folded in the final structure, but aid in preliminary folding steps. Overall pattern is 150 mm square. (Previously published[54])
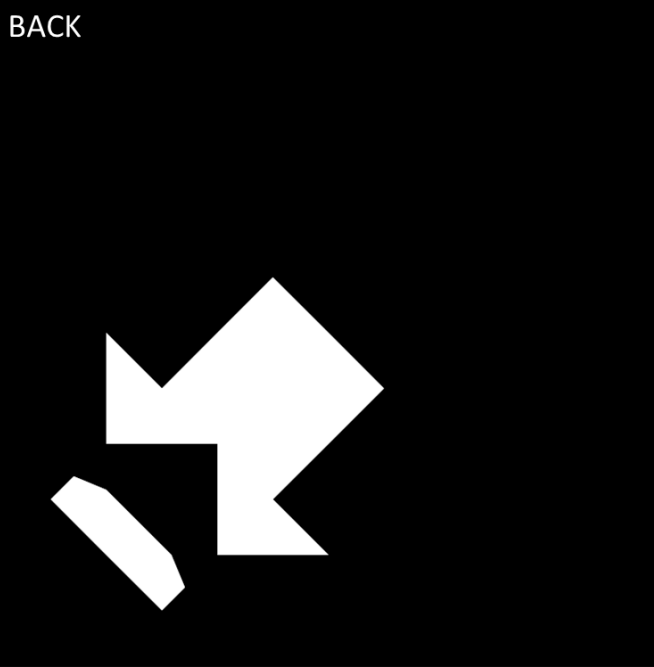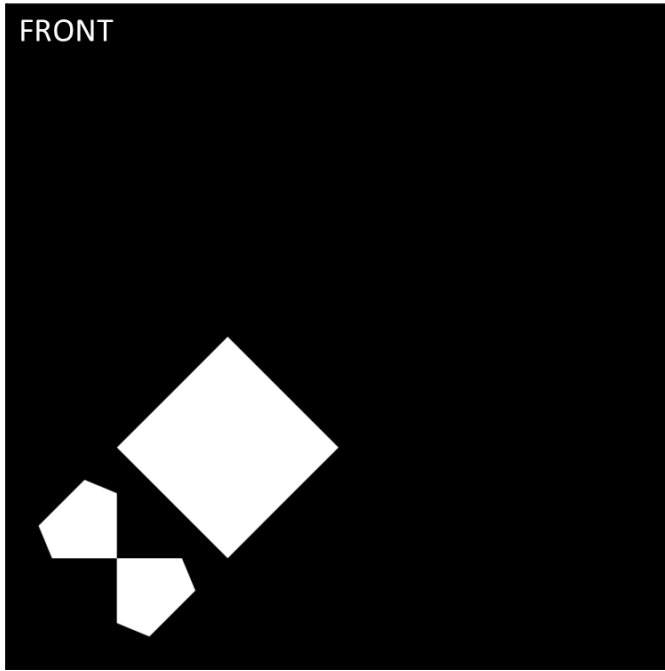
Figure 3-3: Adhesive Application Masks. Masks placed between the origami device and the metal stencil during adhesive application, where the white portions are removed. Masks are 150 mm square. (Previously published[54])
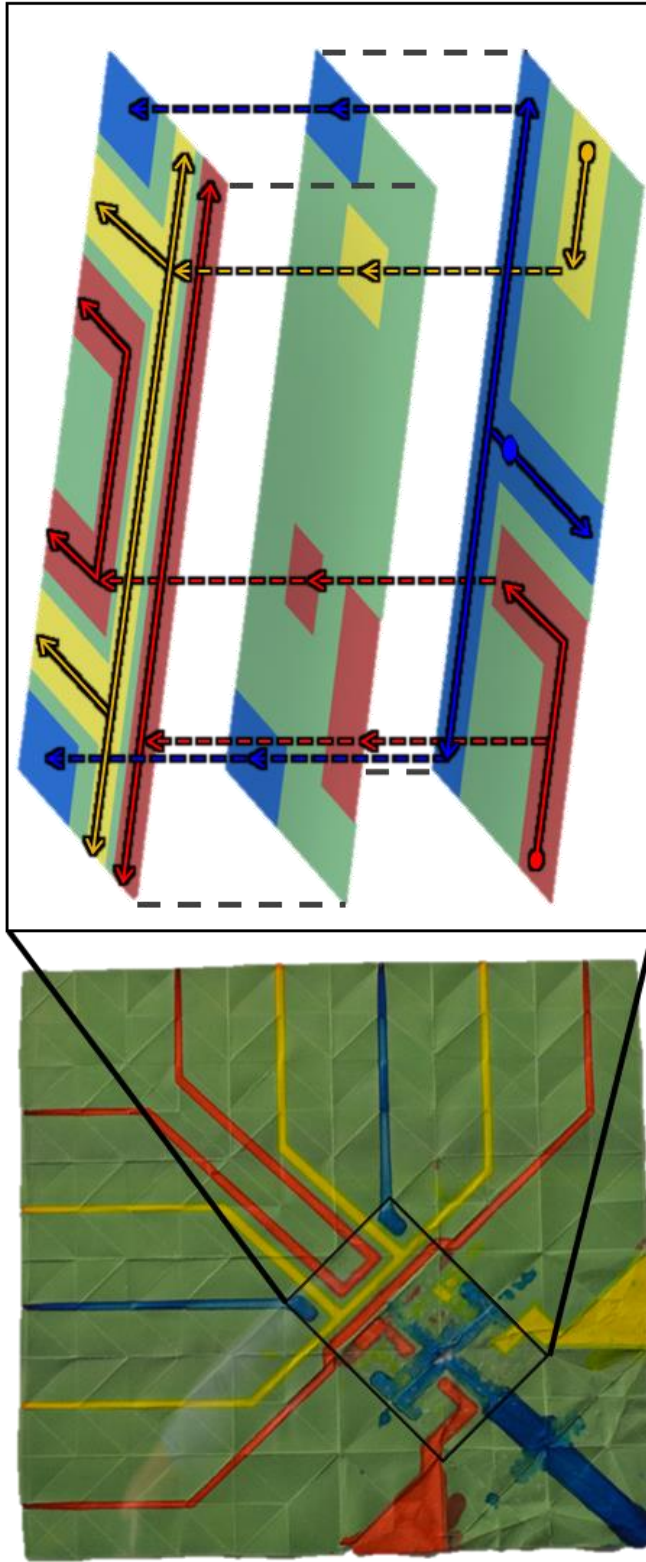
Figure 3-4: Unfolded Origami Peacock. Unfolded peacock post-wicking with a schematic view of how the channels connect when folded. The three colored solutions (Red – allura red, Blue – erioglaucine disodium salt, Yellow - tartrazine) can be seen to have not mixed either inside or outside of the channels in the unfolded peacock. In the callout schematic, dotted gray lines indicate a continuation of paper over folds. Inlets are marked by circles. Arrows indicate direction of flow. (Previously published[54])
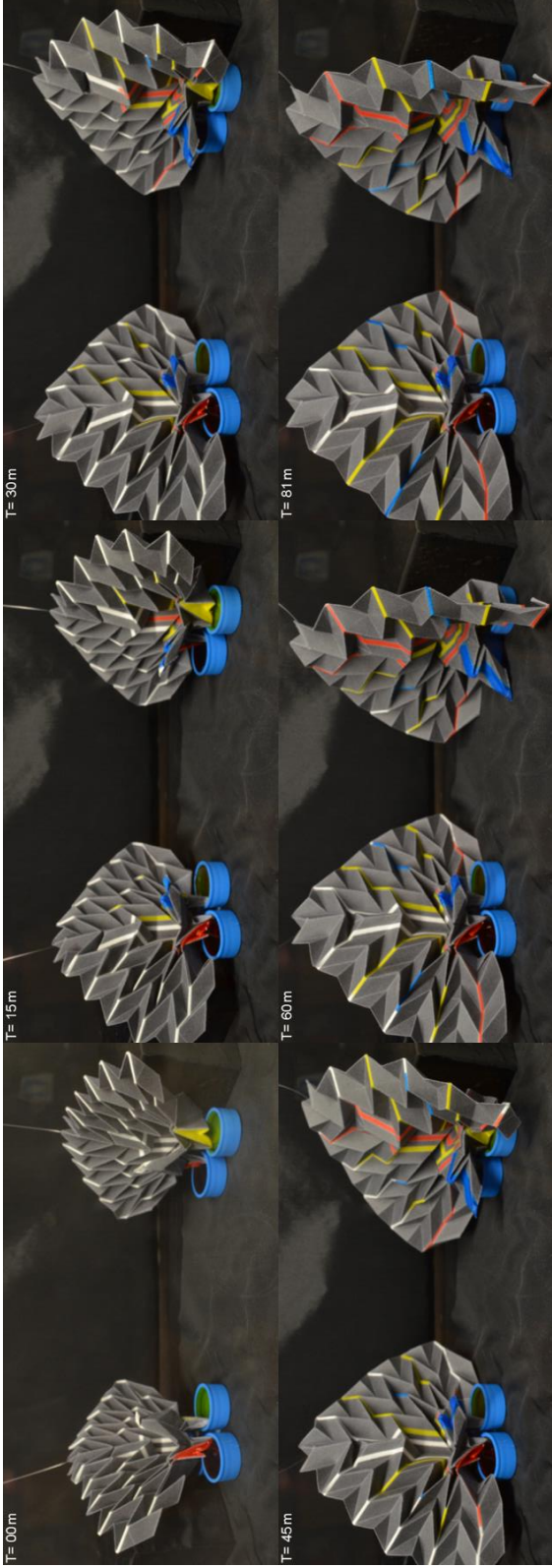
Figure 3—5: Peacock Wicking Time Lapse. Right – peacock held together with uniform adhesive coverage, Left – peacock held together with patterned adhesive coverage (applied through stencil #1). Both peacocks are in sealed humidity controlled chamber kept at >90% RH.

46

Chapter 4: Distance-based Semi-quantitative DNA Detection

INTRODUCTION

Distance-based lateral flow devices promise high resolution, equipment-free quantitative data, without relying on subjective determination of the hue or intensity of a purely colorimetric device. Existing device proposals tailor the detection chemistry, and subsequent device design, to each specific target analyte. Different detection chemistries will require devices to be stored under different environmental conditions, adding logistical complexity to their use.

The goal of this project was to develop a universal detection motif that would work in the same manner, independent of the detection target. The current design solution uses aptamer-coated dyed latex microspheres that combine with the target analyte in a three-component system to form large aggregates. The growth rate of the microsphere aggregates is dependent on the concentration of the target analyte, with higher concentrations leading to more rapid aggregation. Solutions containing these microsphere aggregates will be deposited onto paper, where the smaller aggregates will be able to travel a further distance through the porous microstructure. Larger aggregates will become immobilized more quickly and thus travel a shorter distance. In this way, the distance travelled by the dyed microspheres will be inversely proportional to the concentration of the target analyte. A schematic of this process is depicted in Figure 4-1.

As a proof of concept, a microsphere system using two non-complementary strands of ssDNA[58] were conjugated to two different populations of microspheres. The target analyte was a third ssDNA strand that was partially complementary to both of the other strands.

MATERIALS

1-Ethyl-3-(3-dimethylaminopropyl)carbodiimide (EDC), phosphate buffered saline (PBS), 2-(*N*-morpholino)ethanesulfonic acid (MES), Tween-20, and *N*-Hydroxysuccinimide (NHS) were purchased from Sigma-Aldrich (St. Louis, MO). Whatman grade no. 4 and grade no. 5 filter paper was purchased from Fisher Scientific (Waltham, MA). Hi-Flow Plus 240 nitrocellulose membranes were purchased from EMD Millipore (Billerica, MA). DNA strands [Strand A: 5'-/5AmMC6//iSp18/TTT TTT TTT TCG CAT TCA GGA T-3' Strand B: 5'-TCT CAA CTC GTA TTT TTT TTT T/iSp18//3AmMo/-3' Linker A'-B': TAC GAG TTG AGA ATC CTG AAT GCG-3'] were purchased from IDT (San Diego, CA). Carboxylated blue latex microspheres (.15μm, 1μm, and 10μm) were purchased from MagSphere (Pasadena, CA). Devices were printed using a Xerox Colorqube 8880 printer (Norwalk, CN) and cut out using an Epilog Zing 16 laser engraver (Golden, CO).

METHODS

Preparation of the microspheres

Carboxylated microspheres were conjugated to amine modified ssDNA aptamers. The microspheres were conjugated with either strand A or strand B; the two strands are non-complementary and opposite sense, but both are partially complementary to a third strand, A'-B'.

The 1μm microspheres could be centrifuged during the post-conjugation washing, but the .15μm microspheres did not form compact pellets and were difficult to completely resuspend, so were washed by dialysis.

Hybridization/Wicking Tests

Test strips were designed in SolidWorks and then printed onto cellulose filter paper using wax printing or cut out of nitrocellulose using CO_2 laser cutting.

In each test, excluding controls, microspheres coated with strand A and microspheres coated with strand B were mixed in equal concentrations and amounts to minimize the number of lone, un-aggregated microspheres. At the inlet of each test strip 20μL of solution (5μL of strand A coated microspheres, 5μL of strand B coated microspheres and 10μL of A'-B' linker) was deposited. Solutions were left to sit for varying amounts of time before being deposited onto the test strips in order to determine the speed at which aggregates form.

RESULTS AND DISCUSSION

Solutions containing only microspheres coated with strand A and microspheres coated with strand B did not visibly aggregate over the course of an hour when viewed under a microscope (Figure 4-2), while solutions that contained 100 μM of A'-B' linker showed noticeable signs of aggregation within minutes (Figure 4-3), indicating that the DNA aptamers are likely hybridizing to form aggregate structures.

The cellulose filter papers used, Whatman grade no. 5, has a particle retention size of >2.5 μm. When microsphere-containing solutions are deposited onto filter paper, both the .15 μm and the 1 μm microspheres travel the same distance (Figure 4-4). This is because

filter paper's particle retention size are for flow passing vertically through the paper, not laterally. No change in wicking distance of the 1 μm microspheres was measurable at any linker strand concentration up to 100 μM (Figure 4-5). This indicates that the average lateral pore diameter of the filter papers are likely still too large to prevent the travel of a noticeable number of microsphere aggregates.

Unlike cellulose filter paper, nitrocellulose membranes have a much more homogenous microstructure and have a smaller average pore diameter. When microsphere-containing solutions are deposited onto the nitrocellulose, the .15 μm microspheres travel with the fluid front, while the 1 μm microspheres remain on the surface of the nitrocellulose (Figure 4-6). This is expected behavior, as the average pore diameter of the nitrocellulose membrane is approximately .4μm. What is not expected behavior, however, is that .15μm microspheres that have been conjugated with strand A or strand B travel less than half the distance travel by the unconjugated variety (Figure 4-6). This is also the case for .15 μm microspheres that have gone through a version of the conjugation protocol that does not actually add any ssDNA. The reason for this behavior is not yet known, but is suspected to either be some sort of nonspecific binding or surface charge interaction with the nitrocellulose.

ssDNA conjugated latex microspheres have been previously used in nitrocellulose membranes without issue, so it is expected that these problems are solvable and not an indictment of the proposed detection motif. Further research is required before the viability of the proposed detection technique and its application to real targets can be determined.

FIGURES
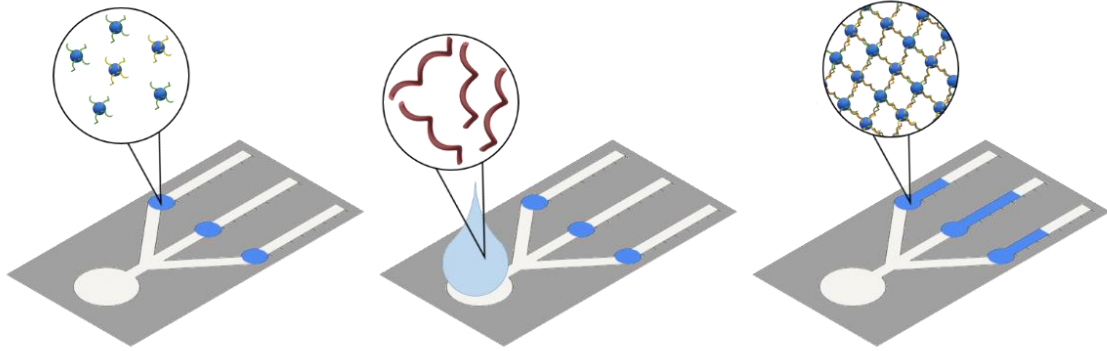
Figure 4-1: Proposed Detection Motif. Two populations of microspheres are conjugated with non-complementary ssDNA that are both partially complementary to a target strand. When the target strand is added, the microspheres aggregate, forming structures larger than the pore size of the paper, preventing further wicking. Multiple sets of microspheres can be predeposited onto a device, each targeted to a specific target.
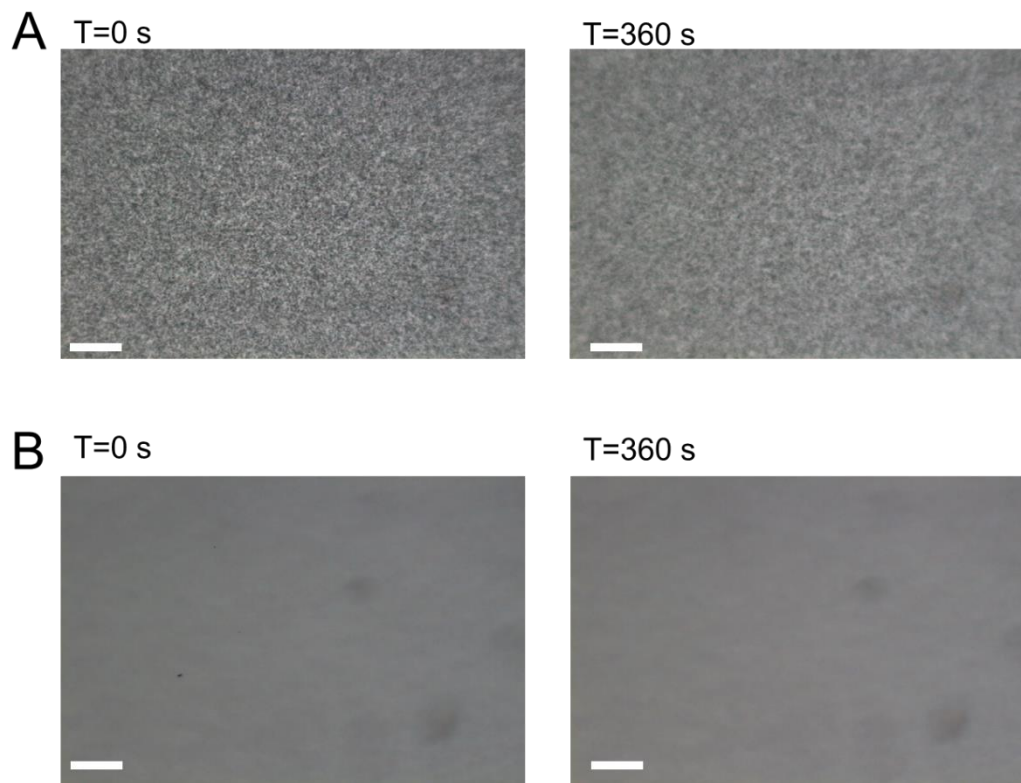
Figure 4-2: Conjugated Microspheres Without Linker. A) 1 μm microspheres (Strand A conjugated and Strand B conjugated) at 1% solid with DI H$_2$O added. B) .15 μm microspheres (Strand A conjugated and Strand B conjugated) at 1% solid with DI H$_2$O added. Images captured immediately after DI H$_2$O was added (T=0) and at T= 360 s. Scale bars are 100 μm.
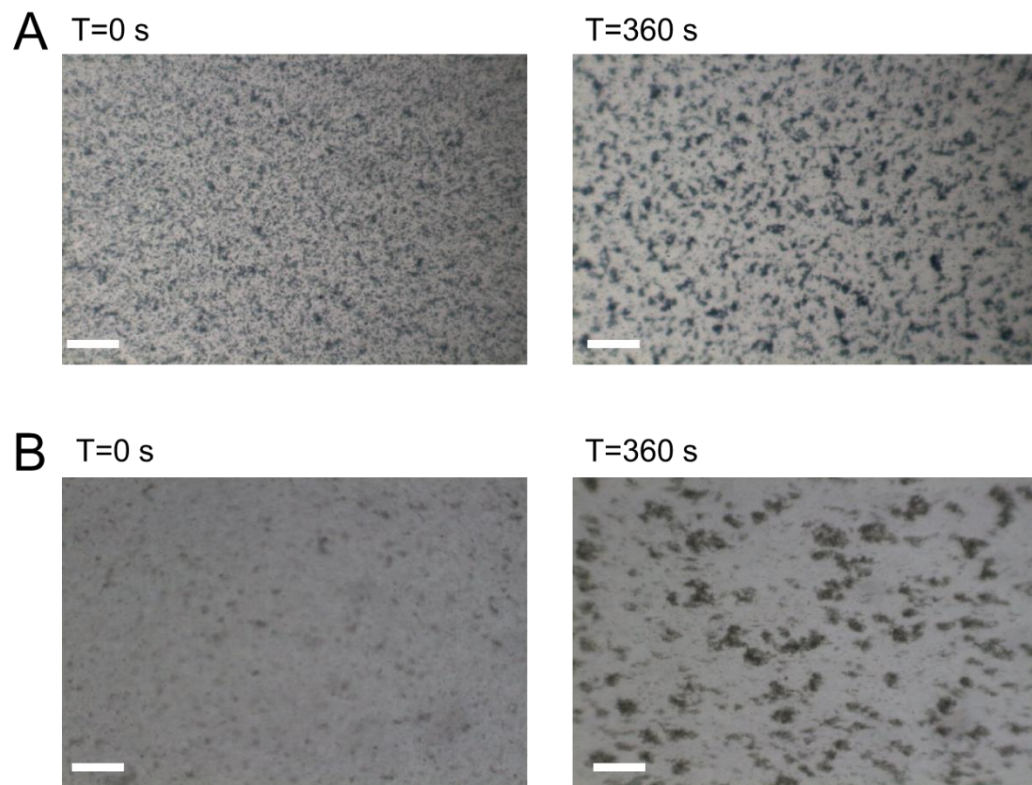
Figure 4-3: Conjugated Microspheres With Linker. A) 1 μm microspheres (Strand A conjugated and Strand B conjugated) at 1% solid with 100 μM A'-B' linker. B) .15 μm microspheres (Strand A c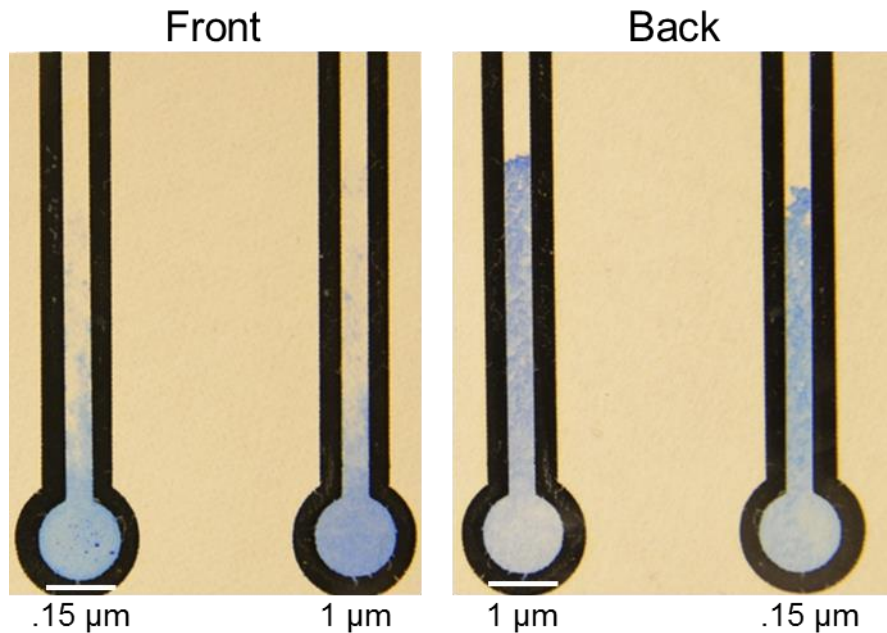onjugated and Strand B conjugated) at 1% solid with 100 μM A'-B' linker. Images captured immediately after linker was added (T=0) and at T= 360 s. Scale bars are 100 μm.

Figure 4-4: Wicking Distance Comparison Between Unconjugated .15 μm And 1 μm Microspheres. Unconjugated microspheres (.15 and 1 μm) in Whatman no. 5 filter paper. 10 μL of 1% solid solution was deposited at the inlet of each channel. Both sizes of microspheres are smaller than the paper's pores and travel approximately equal distances. Scale bars are 5 mm.
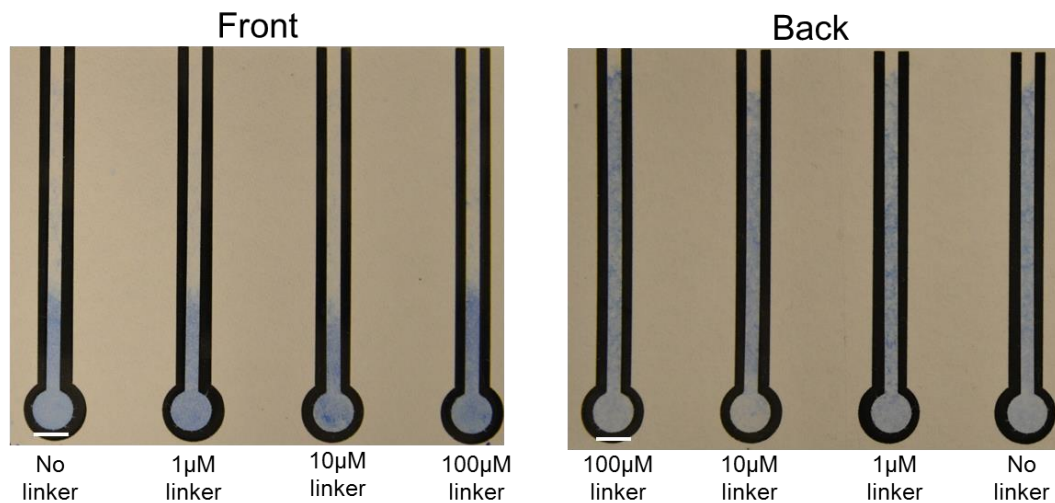
Figure 4-5: Wicking Distance Comparison Between Conjugated 1 μm Microspheres At Different Linker Concentrations. 20μL of 1% solid microsphere solution with the listed concentration of A'-B' linker was deposited at the inlet of each channel. Solution contains equal quantities of microspheres conjugated with Strand A and Strand B. Linker was mixed with the microspheres 60 minutes prior to deposition. Scale bars are 5 mm.
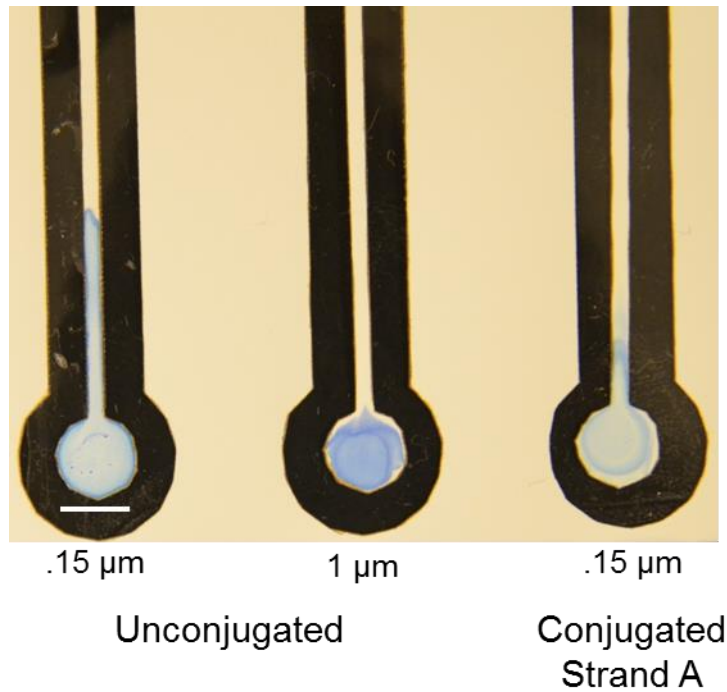
Figure 4-6: Wicking Distance Comparison of Microspheres in Nitrocellulose.
Unconjugated .15 μm microspheres travel with the fluid front through this nitrocellulose
membrane, while the 1 μm microspheres remain on the surface. This is because the average
pore size of the nitrocellulose membrane is only .4 μm. .15 μm microspheres that have been
conjugated with ssDNA travel a much shorter distance through the nitrocellulose than those
that have not been conjugated. The reason for this is still unknown.

REFERENCES

1. V. Gubala, L. F. Harris, A. J. Ricco, M. X. Tan and D. E. Williams, "Point of care diagnostics: status and future", *Anal Chem*, 2012, **84**, 487.
2. X. Li, D. R. Ballerini and W. Shen, "A perspective on paper-based microfluidics: Current status and future trends", *Biomicrofluidics*, 2012, **6**, 11301.
3. D. M. Cate, J. A. Adkins, J. Mettakoonpitak and C. S. Henry, "Recent developments in paper-based microfluidic devices", *Anal Chem*, 2015, **87**, 19.
4. E. Fu, "Enabling robust quantitative readout in an equipment-free model of device development", *Analyst*, 2014, **139**, 4750.
5. H. Kettler, K. White and S. Hawkes, *Mapping the landscape of diagnostics for sexually transmitted infections*, World Health Organization, Geneva, SW, 2004.
6. H. Yagoda, "Applications of Confined Spot Tests in Analytical Chemistry: Preliminary Paper", *Industrial & Engineering Chemistry Analytical Edition*, 1937, **9**, 79.
7. R. H. Muller, "Instrumentation in Microanalysis", *Anal Chem*, 1949, **21**, 427.
8. A. W. Martinez, S. T. Phillips, M. J. Butte and G. M. Whitesides, "Patterned paper as a platform for inexpensive, low-volume, portable bioassays", *Angew Chem Int Ed Engl*, 2007, **46**, 1318.
9. A. W. Martinez, S. T. Phillips, B. J. Wiley, M. Gupta and G. M. Whitesides, "FLASH: A rapid method for prototyping paper-based microfluidic devices", *Lab Chip*, 2008, **8**, 2146.
10. K. Abe, K. Kotera, K. Suzuki and D. Citterio, "Inkjet-printed paperfluidic immuno-chemical sensing device", *Analytical and Bioanalytical Chemistry*, 2010, **398**, 885.
11. K. Abe, K. Suzuki and D. Citterio, "Inkjet-Printed Microfluidic Multianalyte Chemical Sensing Paper", *Anal Chem*, 2008, **80**, 6928.
12. X. Li, J. Tian and W. Shen, "Progress in patterned paper sizing for fabrication of paper-based microfluidic sensors", *Cellulose*, 2010, **17**, 649.
13. X. Li, J. Tian, G. Garnier and W. Shen, "Fabrication of paper-based microfluidic sensors by printing", *Colloids and Surfaces B: Biointerfaces*, 2010, **76**, 564.
14. J. Olkkonen, K. Lehtinen and T. Erho, "Flexographically Printed Fluidic Structures in Paper", *Anal Chem*, 2010, **82**, 10246.
15. W. Dungchai, O. Chailapakul and C. S. Henry, "A low-cost, simple, and rapid fabrication method for paper-based microfluidics using wax screen-printing", *Analyst*, 2011, **136**, 77.
16. E. Carrilho, A. W. Martinez and G. M. Whitesides, "Understanding wax printing: a simple micropatterning process for paper-based microfluidics", *Anal Chem*, 2009, **81**, 7091.
17. Y. Lu, W. W. Shi, J. H. Qin and B. C. Lin, "Fabrication and Characterization of Paper-Based Microfluidics Prepared in Nitrocellulose Membrane By Wax Printing", *Anal Chem*, 2010, **82**, 329.
18. I. Jang and S. Song, "Facile and Precise Flow Control for a Paper-Based Microfluidic Device through Varying Paper Permeability", *Lab Chip*, 2015.
19. S. G. Jeong, S. H. Lee, C. H. Choi, J. Kim and C. S. Lee, "Toward instrument-free digital measurements: a three-dimensional microfluidic device fabricated in a single sheet of paper by double-sided printing and lamination", *Lab Chip*, 2015, **15**, 1188.
20. X. Li, J. F. Tian, T. Nguyen and W. Shen, "Paper-Based Microfluidic Devices by Plasma Treatment", *Anal Chem*, 2008, **80**, 9131.

21. P. K. Anal ChemKao and C. C. Hsu, "One-step rapid fabrication of paper-based microfluidic devices using fluorocarbon plasma polymerization", *Microfluid Nanofluidics*, 2014, **16**, 811.
22. G. Chitnis, Z. Ding, C.-L. Chang, C. A. Savran and B. Ziaie, "Laser-treated hydrophobic paper: an inexpensive microfluidic platform", *Lab Chip*, 2011, **11**, 1161.
23. C. L. Cassano and Z. H. Fan, "Laminated paper-based analytical devices (LPAD): fabrication, characterization, and assays", *Microfluid Nanofluidics*, 2013, **15**, 173.
24. E. M. Fenton, M. R. Mascarenas, G. P. López and S. S. Sibbett, "Multiplex Lateral-Flow Test Strips Fabricated by Two-Dimensional Shaping", *ACS Appl Mater Interfaces*, 2009, **1**, 124.
25. J. F. Nie, Y. Z. Liang, Y. Zhang, S. W. Le, D. N. Li and S. B. Zhang, "One-step patterning of hollow microstructures in paper by laser cutting to create microfluidic analytical devices", *Analyst*, 2013, **138**, 671.
26. E. Fu, S. A. Ramsey, P. Kauffman, B. Lutz and P. Yager, "Transport in two-dimensional paper networks", *Microfluid Nanofluidics*, 2011, **10**, 29.
27. E. Fu, P. Kauffman, B. Lutz and P. Yager, "Chemical signal amplification in two-dimensional paper networks", *Sensors and Actuators, B: Chemical*, 2010, **149**, 325.
28. E. Evans, E. F. M. Gabriel, W. K. T. Coltro and C. D. Garcia, "Rational selection of substrates to improve color intensity and uniformity on microfluidic paper-based analytical devices", *Analyst*, 2014, **139**, 2127.
29. D. M. Cate, W. Dungchai, J. C. Cunningham, J. Volckens and C. S. Henry, "Simple, distance-based measurement for paper analytical devices", *Lab Chip*, 2013, **13**, 2397.
30. W. Dungchai, Y. Sameenoi, O. Chailapakul, J. Volckens and C. S. Henry, "Determination of aerosol oxidative activity using silver nanoparticle aggregation on paper-based analytical devices", *Analyst*, 2013, **138**, 6766.
31. A. Nilghaz, D. R. Ballerini, X. Y. Fang and W. Shen, "Semiquantitative analysis on microfluidic thread-based analytical devices by ruler", *Sensors and Actuators B-Chemical*, 2014, **191**, 586.
32. R. F. Zuk, V. K. Ginsberg, T. Houts, J. Rabbie, H. Merrick, E. F. Ullman, M. M. Fischer, C. C. Sizto, S. N. Stiso and D. J. Litman, "Enzyme Immunochromatography - a Quantitative Immunoassay Requiring No Instrumentation", *Clin Chem*, 1985, **31**, 1144.
33. V. Y. S. Liu, T. Y. Lin, W. Schrier, M. Allen and P. Singh, "Accumeter(R) Noninstrumented Quantitative Assay of High-Density-Lipoprotein in Whole-Blood", *Clin Chem*, 1993, **39**, 1948.
34. Y. Zhang, C. B. Zhou, J. F. Nie, S. W. Le, Q. Qin, F. Liu, Y. P. Li and J. P. Li, "Equipment-Free Quantitative Measurement for Microfluidic Paper-Based Analytical Devices Fabricated Using the Principles of Movable-Type Printing", *Anal Chem*, 2014, **86**, 2005.
35. G. G. Lewis, M. J. DiTucci and S. T. Phillips, "Quantifying Analytes in Paper-Based Microfluidic Devices Without Using External Electronic Readers", *Angewandte Chemie International Edition*, 2012, **51**, 12707.
36. W. Leung, C. P. Chan, T. H. Rainer, M. Ip, G. W. H. Cautherley and R. Renneberg, "InfectCheck CRP barcode-style lateral flow assay for semi-quantitative detection of C-reactive protein in distinguishing between bacterial and viral infections", *J Immunol Methods*, 2008, **336**, 30.

37. K.-K. Fung, C. P.-Y. Chan and R. Renneberg, "Development of enzyme-based bar code-style lateral-flow assay for hydrogen peroxide determination", *Anal Chim Acta*, 2009, **634**, 89.
38. C. Danks and I. Barker, "On-site detection of plant pathogens using lateral-flow devices*", *EPPO Bulletin*, 2000, **30**, 421.
39. D. Y. Stevens, C. R. Petri, J. L. Osborn, P. Spicar-Mihalic, K. G. McKenzie and P. Yager, "Enabling a microfluidic immunoassay for the developing world by integration of on-card dry reagent storage", *Lab Chip*, 2008, **8**, 2038.
40. R. Chen, H. Li, H. Zhang, S. Zhang, W. Shi, J. Shen and Z. Wang, "Development of a lateral flow fluorescent microsphere immunoassay for the determination of sulfamethazine in milk", *Analytical and Bioanalytical Chemistry*, 2013, **405**, 6783.
41. P. Kauffman, E. Fu, B. Lutz and P. Yager, "Visualization and measurement of flow in two-dimensional paper networks.", *Lab Chip*, 2010, **10**, 2614.
42. B. Lutz, T. Liang, E. Fu, S. Ramachandran, P. Kauffman and P. Yager, "Dissolvable Fluidic Time Delays for Automated Paper Diagnostics", 2012, **20**, 788.
43. H. Noh and S. T. Phillips, "Metering the capillary-driven flow of fluids in paper-based microfluidic devices", *Anal Chem*, 2010, **82**, 4181.
44. A. W. Martinez, S. T. Phillips and G. M. Whitesides, "Three-dimensional microfluidic devices fabricated in layered paper and tape", *Proc Natl Acad Sci U S A*, 2008, **105**, 19606.
45. A. W. Martinez, S. T. Phillips, Z. Nie, C. M. Cheng, E. Carrilho, B. J. Wiley and G. M. Whitesides, "Programmable diagnostic devices made from paper and tape", *Lab Chip*, 2010, **10**, 2499.
46. G. G. Lewis, M. J. DiTucci, M. S. Baker and S. T. Phillips, "High throughput method for prototyping three-dimensional, paper-based microfluidic devices", *Lab Chip*, 2012, **12**, 2630.
47. L. Ge, S. Wang, X. Song, S. Ge and J. Yu, "3D origami-based multifunction-integrated immunodevice: low-cost and multiplexed sandwich chemiluminescence immunoassay on microfluidic paper-based analytical device", *Lab Chip*, 2012, **12**, 3150.
48. H. Liu and R. M. Crooks, "Three-dimensional paper microfluidic devices assembled using the principles of origami", *J Am Chem Soc*, 2011, **133**, 17564.
49. L. Ge, J. Yan, X. Song, M. Yan, S. Ge and J. Yu, "Three-dimensional paper-based electrochemiluminescence immunodevice for multiplexed measurement of biomarkers and point-of-care testing", *Biomaterials*, 2012, **33**, 1024.
50. K. M. Schilling, D. Jauregui and A. W. Martinez, "Paper and toner three-dimensional fluidic devices: programming fluid flow to improve point-of-care diagnostics", *Lab Chip*, 2013, **13**, 628.
51. K. Scida, B. Li, A. D. Ellington and R. M. Crooks, "DNA detection using origami paper analytical devices", *Anal Chem*, 2013, **85**, 9713.
52. J. Yan, M. Yan, L. Ge, J. Yu, S. Ge and J. Huang, "A microfluidic origami electrochemiluminescence aptamer-device based on a porous Au-paper electrode and a phenyleneethynylene derivative", *Chem Commun (Camb)*, 2013, **49**, 1383.
53. A. V. Govindarajan, S. Ramachandran, G. D. Vigil, P. Yager and K. F. Bohringer, "A low cost point-of-care viscous sample preparation device for molecular diagnosis in the developing world; an example of microfluidic origami", *Lab Chip*, 2012, **12**, 174.
54. B. Kalish and H. Tsutsui, "Patterned adhesive enables construction of nonplanar three-dimensional paper microfluidic circuits", *Lab Chip*, 2014, **14**, 4354.

55. J. Maekawa, *Genuine Japanese origami*, Dover Publications, Inc., Mineola, New York, 2012.
56. R. Kempaiah and Z. Nie, "From nature to synthetic systems: shape transformation in soft materials", *Journal of Materials Chemistry B*, 2014, **2**, 2357.
57. W. Jung, W. Kim and H.-Y. Kim, "Self-burial Mechanics of Hygroscopically Responsive Awns", *Integrative and Comparative Biology*, 2014.
58. P. H. Rogers, E. Michel, C. A. Bauer, S. Vanderet, D. Hansen, B. K. Roberts, A. Calvez, J. B. Crews, K. O. Lau, A. Wood, D. J. Pine and P. V. Schwartz, "Selective, controllable, and reversible aggregation of polystyrene latex microspheres via DNA hybridization", *Langmuir*, 2005, **21**, 5562.